



University of HUDDERSFIELD

University of Huddersfield Repository

Thongjerm, Piyanud

The study of the effectiveness of Particles in radiation therapy using GEANT4 simulation

Original Citation

Thongjerm, Piyanud (2020) The study of the effectiveness of Particles in radiation therapy using GEANT4 simulation. Doctoral thesis, University of Huddersfield.

This version is available at <http://eprints.hud.ac.uk/id/eprint/35276/>

The University Repository is a digital collection of the research output of the University, available on Open Access. Copyright and Moral Rights for the items on this site are retained by the individual author and/or other copyright owners. Users may access full items free of charge; copies of full text items generally can be reproduced, displayed or performed and given to third parties in any format or medium for personal research or study, educational or not-for-profit purposes without prior permission or charge, provided:

- The authors, title and full bibliographic details is credited in any copy;
- A hyperlink and/or URL is included for the original metadata page; and
- The content is not changed in any way.

For more information, including our policy and submission procedure, please contact the Repository Team at: E.mailbox@hud.ac.uk.

<http://eprints.hud.ac.uk/>

**The study of the effectiveness of
Particles in radiation therapy
using GEANT4 simulation**

University of
HUDDERSFIELD

Piyanud Thongjerm

School of Computing and Engineering
University of Huddersfield

A thesis submitted to the University of Huddersfield
in partial fulfilment of the requirements for the degree of
Doctor of Philosophy

August 2020

Copyright

- I The author of this thesis (including any appendices and/or schedules to this thesis) owns any copyright in it (the "Copyright") and she has given The University of Huddersfield the right to use such Copyright for any administrative, promotional, education and/or teaching purposes.
- II Copies of this thesis, either in full or in extracts, may be made only in accordance with the regulations of the University library. Details of these regulations may be obtained from the Librarian. This page must form part of any such copies made.
- III The ownership of any patents, design, trade marks and any and all other intellectual property rights except for the Copyright (the "Intellectual Property Rights") and any reproductions of copyright works, for example graphs and tables ("Reproduction"), which may be described in this thesis, may not be owned by third parties. Such Intellectual Property Rights and Reproductions cannot and must not be made available for use without the prior written permission of the owner(s) of the relevant Intellectual Property Rights and/or Reproductions.

Abstract

This thesis describes a Monte-Carlo based simulation study in order to investigate the impact of radiation quality especially linear energy transfer (LET) on the damage of living cell induced by radiation. In this study, the simplified target is used for determining the pattern of the energy deposition of charged particles at different energies in macroscopic level by using Geant4 toolkit. This study highlights the factor that may cause the erroneous LET calculation when using small target in the model. It is shown that although LET is used as a universal term to describes radiation quality, its stochastic nature causes uncertainty when incorporating with biological outcome. In addition, the structural DNA model is used to quantify a number of radiation-induced DNA damage in microscopic level by incorporating with spatial distribution of energy deposition. It is important to note that the number of DNA damage is significantly dependent on adjustable parameters in the simulation including energy threshold for inducing the damage. Finally, the experimental database, PIDE, of various cell types and particles allows investigating the factors including type of cell and particle that influence biological effect.

Acknowledgement

Before anyone else, I would like to thank my supervisor, Roger Barlow. Thank you for all your support, guidance and always encourage me to do my research never give up on me. Knowing that your door was always open, and your Skype was always online is such a huge reassurance.

I would like to express my thanks to Thomas Friedrich and his research team for giving access to PIDE database.

I also thank IIAA group members for your helpful advises.

For the financial support, I would like to acknowledge the Royal Thai government. I would not have been able to do my PhD in the UK without this support.

Finally, thank you to my family. Thanks for believing that I could do this, and for endless support. My special thank goes to my partner, Wason, for his unlimited patience, love and especially countless hours of assistance with programming and coding from other side of the world.

Contents

1	Introduction	9
1.1	The Cell	9
1.1.1	The Cell Cycle	9
1.2	Cancer	11
1.2.1	Treatment of Cancer	11
1.3	Radiation Therapy	12
1.3.1	Charged Particle Radiation Therapy	14
1.4	Simulation of Radiation-Induced DNA Damage	17
1.5	Thesis Structure & Hypothesis	18
2	Physical and Biological background	19
2.1	Radiation Damage Modelling	19
2.2	Radiation Physics	20
2.2.1	Interaction of Particles with Matter	20
2.2.2	Energy Loss and Energy Deposition	22
2.2.3	Linear Energy Transfer (LET)	26
2.2.4	Track structure	29
2.3	Radiation Biology	29
2.3.1	DNA structure	29
2.3.2	Direct and indirect effect of radiation	31
2.3.3	Relative Biological Effectiveness (RBE)	32
3	Simulation of radiation quality using Geant4 code	35
3.1	Geant4 and Geant4-DNA code	35
3.1.1	Geant4-DNA	36
3.1.2	Basic setting in Geant4 simulation	36
3.2	Calculation of LET_t and LET_d in the simulation	37
3.3	Distribution of energy deposition	38
3.3.1	LET_d and stepping distance	40
3.4	LET simulation in small target	41
3.5	Why the investigation of LET is interesting and important	42

4	Simulation of direct radiation-induced DNA damage	46
4.1	Orientation of DNA model	46
4.2	Simulation of physical interactions	47
4.3	Production of clusters of DNA breaks	49
4.3.1	Algorithm for identifying energy cluster	50
4.3.2	Calculation of DNA break yield	52
4.3.3	The optimal parameters for DBSCAN for determining energy cluster	53
4.4	Results and model validation	53
4.5	Discussion	55
5	Comparison with data	59
5.1	The PIDE database	59
5.2	RBE and effectiveness	60
5.3	LET	60
5.4	Dose-survival curves	61
5.5	Dependence on cell type	64
5.6	Dependence on particle type	65
6	Conclusion	69
6.1	Conclusion	69
6.2	Future development	70

List of Tables

2.1	Comparison of A-DNA, B-DNA and Z-DNA conformation	33
4.1	An example of an output file of 1 MeV proton obtained from Geant4-DNA	48
4.2	Energy threshold from other studies on the DNA model	54
5.1	Number of experiments provided by PIDE database	60
5.2	Coefficient of parabolic fit of four cell types	65
5.3	Deviation from the straight line for 3 particle types for the V79 sample	67

List of Figures

1.1	A simplified depiction of the human cell structure	10
1.2	An illustration of the cell cycle phases, including the sub-phases of cell division (Mitosis)	10
1.3	TCP/NTCP response curve	13
1.4	Dose distribution of photon, proton and carbon in water	14
1.5	A graphical illustration of a cyclotron-based accelerator facility with one treatment gantry for proton radiation therapy	15
1.6	Experimental proton RBE values as a function of proton energy	16
2.1	A schematic presentation of the principal stages after human cell is exposed to ionising radiation	21
2.2	Diagram illustrating the interactions of proton	22
2.3	The rate of energy loss of protons and alphas	23
2.4	The Landau distribution as a function of λ	25
2.5	The probability density function of ΔE obtained from the Landau distribution that is for 80 MeV proton in 500 μm target	25
2.6	The energy loss as a function of depth for protons of energy 80, 100, 150 and 160 MeV	27
2.7	The plot shows the distance obtained from Geant4 simulation when using different methods and the ratio of the plots	28
2.8	Calculation of track-average LET and dose-average LET	28
2.9	Track structure of proton and alpha particles	30
2.10	Nucleotide	31
2.11	Structure of DNA	32
2.12	Structure of DNA in different conformation	33
2.13	Structural parameters of B-DNA conformation	34
2.14	Direct and indirect damage to a DNA strand	34
3.1	Standard Geant4 and Geant4-DNA extension simulation	36
3.2	Definition of step length and energy deposition in Geant4	38
3.3	Geometry of energy deposition simulation	39

3.4	The plot of 80 MeV proton shows: a) histogram of a total length made by a particle track in the small slide of the volume b) the relationship between energy and dose deposited in the target c) the distribution of LET_t d) the distribution of LET_d	40
3.5	The ratio of the plots of the distribution of LET_t and the distribution of LET_d shown in figure 3.4	41
3.6	Energy deposition by simulated 150 MeV protons in a slice of water of thickness 0.5 mm, 1 mm and 2 mm	42
3.7	LET_t (lines) and LET_d (crosses) as a function of depth from Geant4 simulations of 150 MeV protons travelling through water in slices of 0.5 mm (black), 1 mm (red) and 2 mm (blue)	43
3.8	LET_t and LET_d of proton at a) 80 MeV, b) 100 MeV and c) 150 MeV as a function of depth	44
3.9	The averaged LET_t in a 10 μm target	45
3.10	Dose of a primary proton and alpha as a function of LET_t (keV/ μm)	45
4.1	Organisation of DNA model in the cell nucleus target	47
4.2	The chromosomes territories of an fibroblast 18 cell nucleus models	47
4.3	Dimension of cell nucleus in the cell model	49
4.4	Positions of individual proton	50
4.5	Illustration of a) the effect of distance as a defined parameter in DBSCAN algorithm	51
4.6	Example of varying the energy threshold in DBSCAN algorithm	52
4.7	Illustration of DNA strand break definition	53
4.8	Dose of a single track of particle	55
4.9	Number of particles for 1 Gy	56
4.10	Number of DNA break from a single track of proton and alpha particle	57
4.11	Total DNA double strand breaks	58
5.1	Calculated and given LET values	61
5.2	Four experimental data of the 954 datasets from PIDE database	62
5.3	The difference of linear and quadratic fit through survival fraction and delivered dose of V79 cell data sets	63
5.4	Fitted and quoted values of β , taken from the PIDE database	64
5.5	Fitted values of the negated slope plotted against the LET obtained from the Bethe-Bloch formula	65
5.6	The parabolic fit of ABE as a function of LET (keV/ μm) of V79, T1, C3H10T1 and NB1RGB cells	66
5.7	The ABE values of V79 cells as a function of LET	67
5.8	The ABE values of V79 cells as a function of LET (LET is restricted to 100 keV/ μm)	68
5.9	Histogram of three different particles showing the deviation of the points from the straight regression line in figure 5.8	68

Chapter 1

Introduction

The following thesis explores the effectiveness of charged particle radiation therapy through simulation. This introductory chapter provides context for the technology and discusses the biological rationale for radiation therapy - especially charged particle therapy - at a cellular level as well as the advantages and known uncertainties of treating cancer with high energy ionising radiation. For the purposes of understanding the current effectiveness of radiation therapy, in particular radiation-induced cell damage, a model has been developed within the well-recognised and thoroughly validated Geant4 particle-matter interaction code[1]. A brief introduction to the Geant4 code and processes of the developed model will be also given in the following chapters.

1.1 The Cell

Cells are the most fundamental structural units of all living matter. All known organisms, including the human body itself, are made up of these microscopic building blocks. Human cells are comprised of a cell nucleus, which contains the majority of the cell's genetic information, *i.e.* deoxyribonucleic acid (DNA), surrounded by a mass of cytoplasm (a solution of water, salts and proteins) and mitochondria, all externally bound by a bio-membrane, see figure 1.1. Note that this is a simplified description of a cell, however for the purposes and context of this thesis a more detailed description of the cell structure and functions is not required.

1.1.1 The Cell Cycle

As a cell grows and divides naturally it undergoes a cycle of four steps: Step 1, the so-called Gap or Growth phase, in which the cell increases in size and its cellular contents are duplicated; Step 2, Synthesis, in which the DNA is replicated; Step 3, another Gap/Growth phase, in which the cell prepares for division; and Step 4, Mitosis, wherein the cell separates into two identical so-called daughter cells.

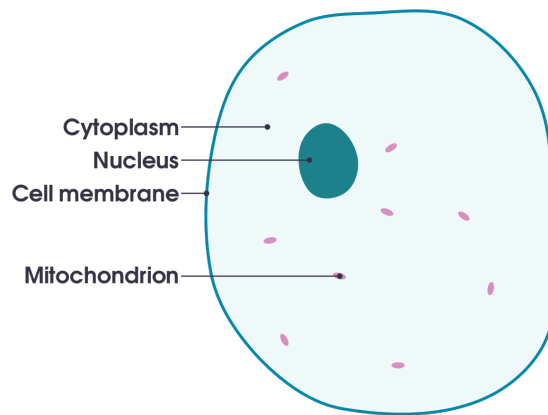


Figure 1.1: A simplified depiction of the human cell structure [2]

The process of Mitosis has unique sub-phases: Prophase, in which the nucleus membrane breaks down and spindle fibres form; Metaphase, in which the spindle fibres attach to and align the cell chromosomes; Anaphase, in which the cell's duplicated contents migrate to opposite ends of the cell; the Telophase, wherein new membranes appear around two separate nuclei; and finally, Cytokinesis, in which the cell splits into two identical daughter cells. The cell cycle is illustrated in figure 1.2.

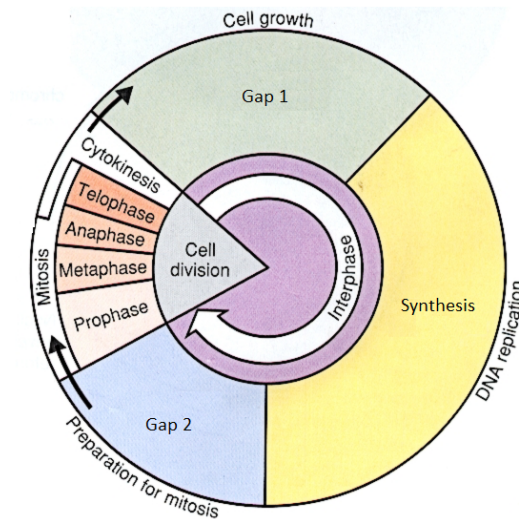


Figure 1.2: An illustration of the cell cycle phases, including the sub-phases of cell division (Mitosis) [3]

Throughout the cell cycle, there is a number of so-called checkpoints in which the DNA or chromosomes are checked for damage or misaligned, respectively.

DNA damage checkpoints occur at each Gap phase. Chromosome alignment is checked in the Mitosis Metaphase. Failure to pass these checkpoint will result in the subsequent cell cycle phase being delayed for the damage to be repaired. If the DNA is irreparable, the cell may enter a state of Apoptosis, sometimes known as cell death, in which the cell loses water and the nucleus shrinks and fragments to the point of destruction. Cell cycle checkpoints and Apoptosis ensure that only healthy cells are replicated to prevent mutation or abnormal growth.

1.2 Cancer

When the cells grow abnormally it can form a lump, called a tumour. For non-cancerous cell, it is called benign tumour which does not invade surrounding tissue or spread to other areas of the body. However, it can be dangerous when it is growing very large, pressing nearby tissue and organ even blocking blood vessels.

Malignant tumour is cancerous cell in which the growth and division phases of cell cycle continue to take place even when the cell contains damaged DNA and would normally have failed at a given checkpoint. This process may occur for a number of reasons, which is why cancer as a pathology encompasses a great number of diseases. Notably, there are more than 200 cancer types which are defined by either the primary site or the type of cell it started from.

An individual is said to have cancer, if the process of abnormal cell division continues uncontrollably. These abnormal cell masses can invade and destroy normal cells and/or adjacent organs. Some particularly volatile cancers may even spread from the primary site to other parts of the body in a process called metastasis.

Benign tumour does not usually recur once treated or surgically removed unlike malignant tumour. Therefore, it is challenging to treat or kill cancer cells without harming the rest of the body.

1.2.1 Treatment of Cancer

There are many treatment methods for cancer, including surgery, in which the tumour is physically cut from the patient, chemotherapy, in which the patient is intravenously provided strong chemicals which will kill the cancerous cells, or a combination of them both. However, different types of cancerous cells respond differently to the various methods. For example, some cancers may not be susceptible to chemotherapy and the side effects are too risky and/or surgical removal would be too invasive and likely fatal. As a result, radiation, *i.e.* the process on bombardment of photons (X-rays) or relatively high-energy, particles as treatment for cancer has certain advantages as it is non-invasive and has shown to have less systematic side effects when compared to chemotherapy. It also enables localised treatment preventing damage to the surrounding health tissue. The rationale of radiation therapy and current studies in this area are discussed in the following

section 1.3.

1.3 Radiation Therapy

Radiation therapy is a treatment method for cancer in which a photon or relatively-high energy charged particle beam is focused to a treatment target. An ionising beam can either interact directly with a local DNA strand or indirectly produce free radicals after ionising water molecule inside the cell. Due to these interactions, it can cause the strand to break causing irreparable damage and, after prolonged exposure, tumour cell death. The further detail of the interaction is given in the section 2.3.2.

DNA damaging by ionisation radiation is a non-selective process. As a result, damage will not only occur in tumour cells, but also healthy cells in the radiation pathway as the beam penetrates through normal tissues before reaching a planned target depth. Today, most research and development surrounding radiation therapy focuses mainly on conforming appropriate radiation doses for specific cancerous cell types, while minimising the dose applied to surrounding healthy tissues. Therefore, dose distribution across the target is one of the most crucial factors in radiation therapy being a viable treatment method.

When prescribing radiation dose for a target tumour, an important factor to consider is the ratio of probability of tumour eradication or so-called tumour control probability (TCP) and normal tissue complication probability (NTCP). It represents the relative damage to cancerous tissue compared to the damage in nearby healthy tissue. As depicted in figure 1.3, El Naqa et al. show that a viable therapeutic ratio can be obtained in the situation where a high response probability of TCP is maintained while minimising the NTCP [4]. A high TCP can be achieved by improving the precision of the beam delivery technique.

To further minimise the NTCP it is also common practice for a tumour to be irradiated multiple times over multiple days at lower dose. This allows for the accumulation of the required dosages for probable cell death, while allowing any minor damage incurred to surrounding healthy tissue time to heal. The process is known as dose fractionation. For future reference, the dose received by a patient in a single session is denoted dose/fraction.

There is a number of common radiation therapy methods surrounding the use of either photons, protons or carbon ions. Photon radiation therapy is the most widely used radiation treatment method and is available at most of cancer treatment centres. The beam can be generated by using linear accelerator to accelerate electrons and collide those electrons with a high atomic number target, such as tungsten or molybdenum. The frequency of photons emitted, *i.e.* the X-ray spectrum, depends on the target material and accelerating voltage. When a photon beam hits a target similar to human tissue, such as water (this is the case due to cytoplasm comprising the majority of a cell, the majority of which is water), energy deposition hits a peak within only a few centimetres from the target surface after a short build-up period.

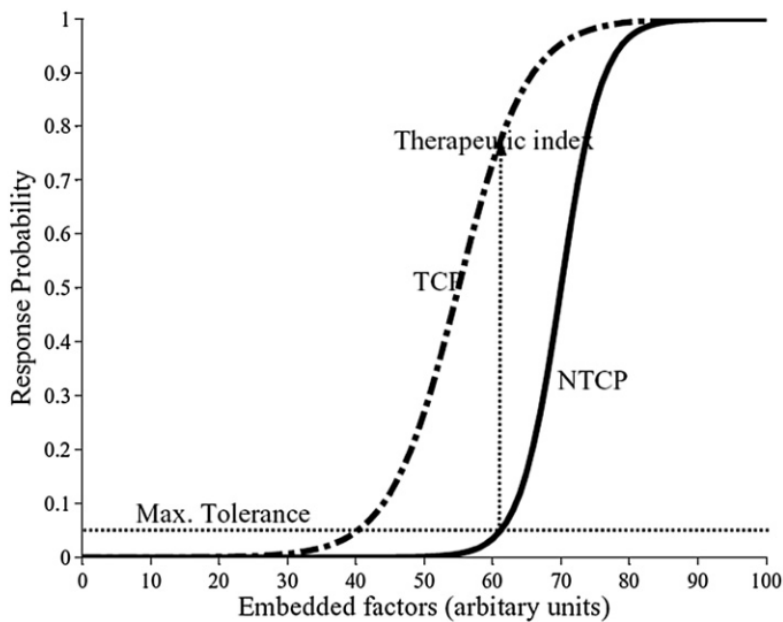


Figure 1.3: The response curves of TCP and NTCP for a given dose distribution shows the response probability as a function of weighting factors which refer to equivalent dose units [4].

Energy deposition subsequently decreases exponentially with a relatively-low decay constant. As a result, if a target tumour is located more than a few centimetres from the target surface, significant damage may have to be accepted in the health tissue near the skin surface such that sufficient dosages are achieved at the target penetration depth. Moreover, even if the tumour is located only a few centimetres from the target's surface, significant damage may be caused to tissue or organs beyond the tumour location due to the exponential decay.

The interaction of charged particles with human tissue is markedly different to that of photon-tissue interaction, as some stages of the cell cycle described in figure 1.2 are more radiation resistant than others. Charged particles interacting with matter deposit only a small percentage of their energy as it propagates until suddenly depositing almost all of the remaining energy just before a given penetration depth which is proportional to the initial particle energy, see figure 1.4. This characteristic results in a unique peak in the dose distribution. This peak is known as a *Bragg peak*. Note that charged particles distributions have a tail following the sharp decay after the Bragg peak. This is due to secondary scattering as a result of direct nuclear interactions with atomic nuclei.

Overall, when solely considering the dose distribution curves, it is clear that charged particle radiation is a much more practical option for treatment of tumours in which the surrounding tissue is particularly sensitive in nature, *e.g.* brain tumours. Unfortunately, the systems required to accelerate protons or heavy ions to

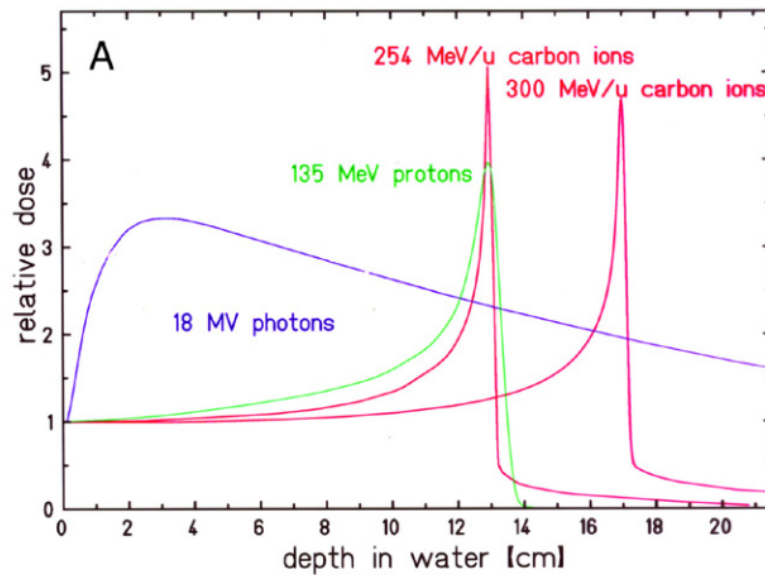


Figure 1.4: Dose distribution of photons, protons and carbon ion as a function of depth in water (cm). Multiple beam energies are shown for carbon ion [5].

sufficient energies are significantly larger, more complex and more expensive than equivalent X-ray machines. This leads to the discussion of the technologies and challenges associated specifically with charged particle radiation therapy.

1.3.1 Charged Particle Radiation Therapy

In recent years, the interest in treating cancers with charged particle beams has significantly increased because of its benefit over conventional therapy as it gives sharp dose distribution. Therefore, the radiation dose to healthy tissue outside a treatment target area could be reduced that allows sparing of surrounding cells when delivering the proton beam precisely to the target. However, to produce sufficient accelerating energies, large and/or expensive particle accelerators such as synchrotron, cyclotron must be used. An illustration of the cyclotron-based proton therapy accelerator facility with one treatment gantry is depicted in figure 1.5. Note that, although still a prominent issue, the cost for such systems has reduced significantly in the last decade and since 2010 over 30 proton therapy facilities have been installed around the world, most notably, a synchrotron-based facility (4 treatment rooms) at the Mayo Clinic (private), Rochester, US, installed 2016, and an state-funded (UK National Health Service (NHS)) cyclotron-based facility (3 treatment rooms) at the Christie Hospital, Manchester, UK, installed 2018. Moreover, due to recent successes, there are at least fourteen more facilities are under construction and already planned for installation in the next 2 years in the USA and UK alone [6].

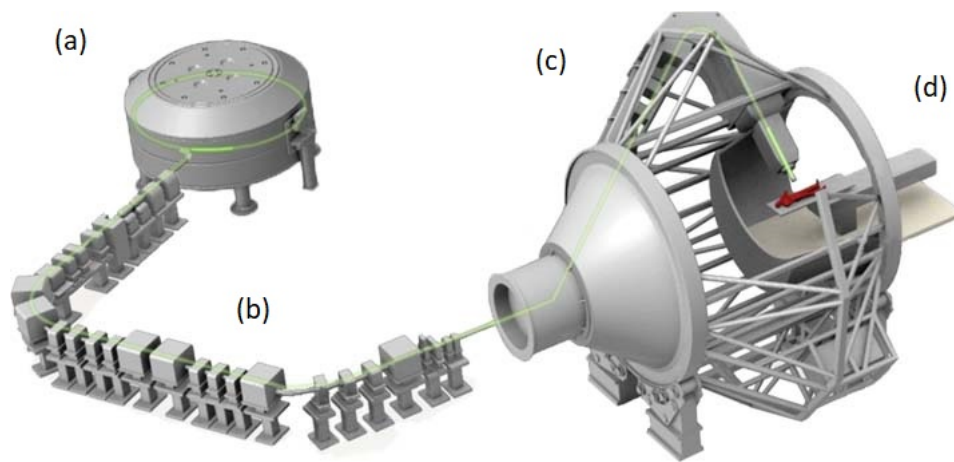


Figure 1.5: A graphical illustration of a cyclotron-based accelerator facility with one treatment gantry for proton radiation therapy. The system comprises (a) a cyclotron proton accelerator magnet system (b) a magnet beamline for focusing the proton beam (c) a manoeuvrable (six-degrees of freedom) gantry for precision beam delivery to the patient. An adult human is depicted in red for scale (d) [7].

Prescription of proton radiation treatment for a given tumour varies depending on many factors including radiosensitivity of type of cancer cell and cell cycle. As a result, defining dosages for each case requires planning based on clinical experiences. This is because the biological effect from the beam is not simply related to a given dose. In addition, consequences after irradiation differ between treatment type, *e.g.* protons treatment may have more negative side-effects on a patient than carbon ions treatment would have due to their unique circumstances. As a result, mass-adoption of charged particle therapy to treat cancer is being held back by a lack of detailed understanding of the relationships between physical beam properties and biological outcome.

When considering biological effects between radiation, relative biological effectiveness (RBE) is used to represent the effectiveness of radiation as it is a ratio of the outcome for a given radiation of choice with respect to a reference x-ray beam producing the same radiation-induced cell damage. A concern is that a constant RBE of 1.1 for proton beam has been used in a clinical setting at some cancer centres. This RBE of 1.1 is considered reasonable for all initial energy levels, dose/fraction and tissue type [8]. However, in reality the RBE is not only a variable with respect to beam parameters such as energy, but also shows non-linear relations. Paganetti showed the variation of RBE arising from dose/fraction, cell type and initial energy in both *in vitro* and *in vivo* studies [5]. Figure 1.6 shows the *in vitro* study of the RBE for cell survival irradiated with proton beams of less than 8.7 MeV. It is clear that, at lower energies, proton beams although more effi-

cient in inducing cell death within tumour cells, also induces significant damage to adjacent healthy cells.

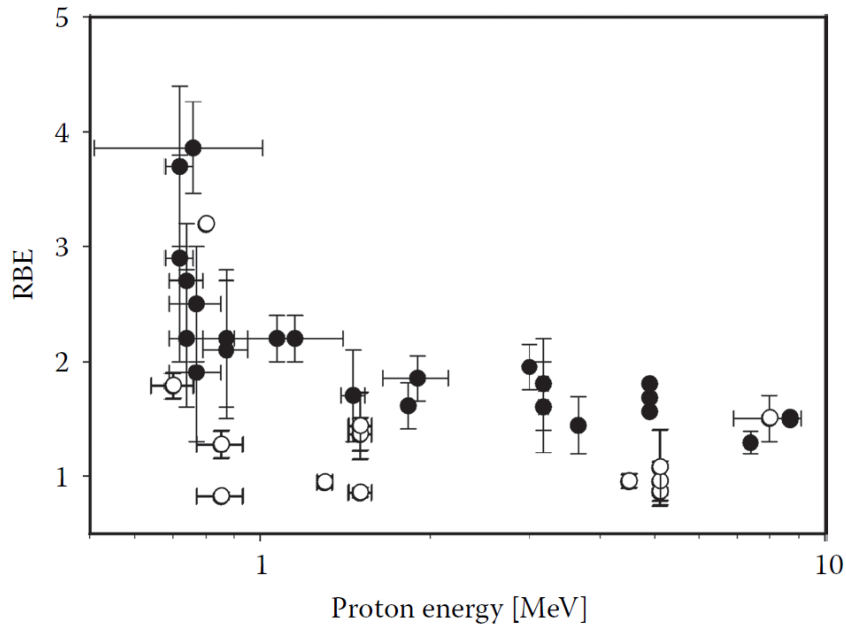


Figure 1.6: Experimental proton RBE values as a function of proton energy. Closed circles show RBEs for dose greater than 4 Gy, open circles show RBEs for doses less than 4 Gy [5].

When considering the biological outcome of radiation on cells, in almost all cases, DNA is considered as the most critical target for damage because it carries essential genetic information for cell proliferation and replication [4, 9]. It is also well-known that higher energy deposition in the cell nucleus increases the chance of damaging cells [10]. However, many questions remain unanswered because the correlation between physical interactions and biological mechanisms which repair damage or induce apoptosis are unknown. An example of such a complexity would be a double strand break (DSB) repair mechanism. For a case in which two adjacent DNA strands are broken (DSB), and apoptosis is not induced (common in cancerous cells), the cell may repair itself by reconnecting the broken strands in a different configuration, resulting in cell mutation. Such complexities may have unforeseen detrimental side-effects. As a result, it is important that a practicing radiation therapist has a full understanding of the probable outcome for a given patient-treatment plan. Notably, it is this question of uncertainties in knowledge surrounding physical interaction-biological outcome which presides over this thesis as a whole. However, in the absence of potentially unethical clinical trials, to further understand such complexities in a safe environment one must explore such correlations through simulation.

1.4 Simulation of Radiation-Induced DNA Damage

There are several approaches to investigate the interaction of ionising radiation with living cells and in determining probable cell damage. These include simulation (analytical or numerical) and biological approaches. Biological experiments for investigating the effects of ionising radiation have significant limitations in that certain experiments may be impossible, unethical, etc and biological experimentation has an inherently large variance in results from one study to another. Simulation allows examination in various, even extreme or unlikely, conditions. Moreover, numerical models allow for probabilistic outcomes to be iteratively simulated in order to produce reliable statistics. As a result, for the purposes of exploring charge particle-DNA interactions a semi-analytical model has been developed in Geant4, implementing both physical and biological processes.

It should be noted that the RBE (biological outcome) can be derived from various perspectives. In a lab-based experiment, various types of cell are exposed to ionising beam under different conditions. These cells then will be analysed by using gel electrophoresis, which is a gold standard technique, in order to determine cell survival after irradiation. In this case, the outcome would be determined by the cell survival rate. However, it is not as straightforward to assess cell death from a Monte Carlo-based study as modelling full cells and the complex mechanisms therein would be difficult to reproduce in the simulation. As a result, biological outcome will be determined at a sub-cellular level and represented by number of DNA strand break instead.

To date, studies in this area attempt to use Monte Carlo simulation codes to model incident particles transporting to and interacting with a biological target in order to predict the mechanism involved. Many research groups have developed the simulation codes for this purpose, including KURBUC, PATRAC, and Geant4. Although all three have been shown to have good agreement with experimental data, KURBUC and PATRAC are in-house programs and are not accessible for external users. In contrast, Geant4 is an open-source toolkit with which users can develop their own applications allowing the validation of simulated results among research groups and communities. As a result, the model constructed for this study was implemented in Geant4.

The simulation of radiation-induced DNA damage can be done in several different ways. Notably, previous studies have tended to assume damage outcomes based on a simplified target representing biological unit such as a single cell or DNA strands or even simply water. The model has no fixed molecular or cellular structure defined. Rather, advancing on a method pioneered by Francis *et al.* [11], a randomised target volume with non-homogenous properties is generated and the algorithm randomly scores the location of the damage according to the local energy deposition. In this case, it saves the simulation time as it does not take into account the structural complexities structure of DNA.

The approach of simulating DNA in its entirety allows one to examine the spatial distribution of interaction at the level of DNA molecules and small discrete

units of a cell. The simulation would also include a detailed structure representing small units of individual DNA strands, enabling the investigation of the physical interaction and subsequent production, scattering and secondary interaction of hydroxyl radicals, produced by process of water radiolysis, around the DNA structure. However, the limitation of this method is the significant computation expense (order of weeks per simulation). This approach can be found in the works of Meylan *et al.* and Lampe *et al.* [12, 13].

1.5 Thesis Structure & Hypothesis

This thesis explores the biological effectiveness of charged particle radiation therapy, focusing on furthering understanding of the correlation between physical beam-tissue interactions with probable biological outcomes. The chapter structure follows: Chapter 1: Introduction; Chapter 2: Physical and Biological Background; Chapter 3: Simulation of Radiation Quality Using Geant4; Chapter 4: Simulation of Direct Radiation-Induced DNA Damage; Chapter 5: Comparison of Results With Experimental Data; Chapter 6: Conclusions and Further Work.

The working hypothesis of this thesis is that the different charged particle with the same Linear Energy Transfer (LET) may give different biological outcome as the pattern of energy deposition of each particle is unique to its physical properties.

Chapter 2

Physical and Biological background

In this chapter, the physics and biology of ionising radiation-living tissue interactions will be discussed in more detail. Furthermore, this chapter also outlines the characteristics of proton and ion beams and reviews, based on previous studies, the manner in which these characters have an impact on the outcomes of radiation therapy.

2.1 Radiation Damage Modelling

Radiation damage to a biological molecule occurs when ionising radiation physically interacts with the molecule by transferring its energy through excitation or ionisation. The development stages of damage can be discussed in terms of early damage, in the first 10^{-12} seconds, mid-term, within the first few hours, and late consequences, within days or years after a cell is exposed by radiation. The timeline of this damage is shown in figure 2.1. Notably, there are many studies which utilise these principal stages of radiation damage as a framework for developing the radiobiological model. In the early stage, energy deposition can be as a result of either direct interaction with the molecules of the medium or indirect interaction from secondary scattered reactive radicals diffusing to the target. This process may cause DNA strands to break and consequently trigger cell repair system or apoptosis/cell death depending on the complexity of the damage. Assuming repair mechanisms are induced, a number of issues may arise such as chromosome aberration, mutation due to alter DNA strand configurations and/or alteration of cell cycle leading to the damage at the cellular level. The effects induced by ionising radiation can be observed shortly after irradiation at a macroscopic scale such as tissue damage causing radiation burn or acute radiation syndrome. It is important to note that where cell death is not induced, repair mechanisms induced on cells may increase risk of long-term effects, including the possibility of secondary cancer which may appear days or even years later. Eventually, both early and late

side-effects would result in organ damage. The likelihood of the damage is related to the dose of radiation.

Radiobiological models are constructed to study the impact of radiation at the cellular level to help understand the mechanisms and processes at a microscopic level by implementing radiation physics and validating the results against biological experiments. Following validation, such a model may be used to explore various unique scenarios to predict probable biological outcomes with biological experimentation. Other approaches may look at the bigger picture, macro-scale, such as NTCP/TCP models, which are developed based on the clinical outcome experience and experimental data. These models use cell survival rates as a method for predicting biological outcomes.

This thesis focuses on the development and use of a radiobiological model for investigating the impact of spatial dose distribution of radiation in cell molecule. Understanding how the resultant distributions vary for given parametric changes will help further understanding regarding radiation and biological outcomes.

2.2 Radiation Physics

2.2.1 Interaction of Particles with Matter

When a particle propagates through the medium, it eventually interacts with one of medium atoms. However, the physical processes involved in a given interaction are determined by the type of incident particle. This section discusses the interaction of radiation according to the physical properties of a photon (neutral charge) and charged particles. Both types of radiation have been used widely in radiation therapy, however, the principle of implementing either neutral or charged ionising radiation is unique in term of dose distribution, see figure 1.4.

Photon

The photon interaction with medium atoms is classified as indirect ionising in that it interacts with the atom electrons, transferring its energy to the electron and is subsequently absorbed. These higher-energy electrons may break from the atom orbit and scatter such that they have further interactions with adjacent atoms in the absorbing material. There are three main processes as a result of the energy absorption of the ionising photon: the photoelectric effect, Compton scattering, and pair production. These processes each depend on the initial energy of the photon, usually X-ray, or primary beam. Compton scattering dominates in radiotherapy because photon beam energy is typically in the intermediate energy range from 100 keV to 10 MeV [14]. In this process, the incident photon gives part of its energy to the atomic electron as kinetic energy and then deflects from its original trajectory, propagating further into the medium with lower energy, with the process repeating until absorption. When human tissue is irradiated with high energy photons, scattered electrons within the tissue can initiate a destructive biological process,

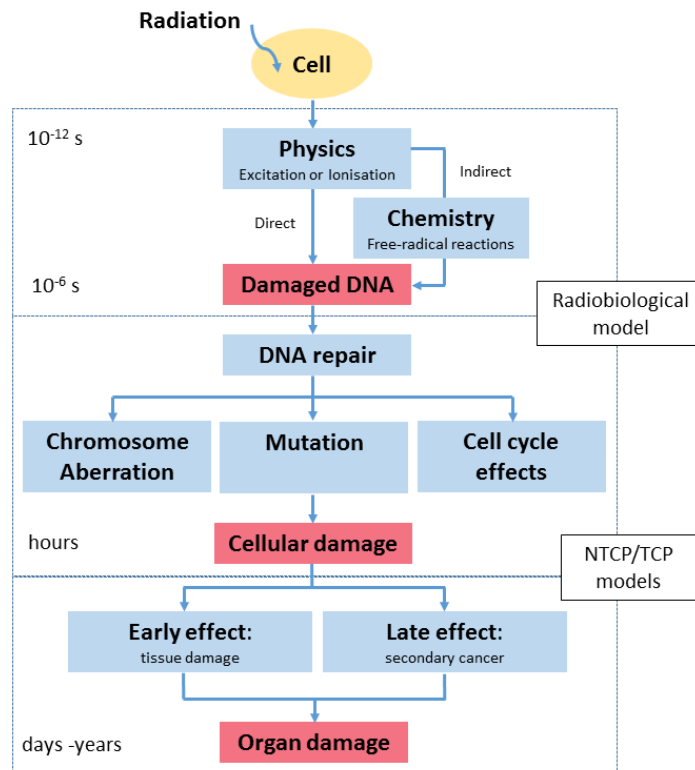


Figure 2.1: A schematic presentation of the principal stages after human cell is exposed to ionising radiation. The approximate time course is indicated for each process. The important task is to characterise each stage to be able to make a mechanistic description of the radiation effect in the human cell or tissue. Such a model facilitates selecting optimal radiation therapy and paves the way for the estimation of genetic and cancer risk factors in humans.

breaking chemical bonds of vital structures within cells. The detail of chemical and biological interaction is discussed in further section.

Charged Particles

Heavy particles, *i.e.* those with relative significant mass, interact directly with medium atoms. Protons and other heavy ions can interact with both orbital electrons (inelastic scattering) and/or the atomic nuclei (indirect elastic/direct inelastic scattering). The physical collision and subsequent scattering is as a result of the Coulomb force interactions between the electric field of the incident particles and the electric field of the electrons or atom nuclei. Figure 2.2 illustrates a proton interaction. The incident particles lose their energy in incremental steps along their path when interacting with the material. In principle, heavy ions are more likely

to scatter with negligible loss of energy because they are more massive compared to those electrons which experience greater multiple scattering. When the particle energy increases, the probability of nuclear disintegration will also increase. The direct interaction of incident heavy charged particles with atomic nuclei also produces radioactive nuclides. In proton therapy, the short-lived radioisotopes produced after the beam interacts with tissues are also useful for radiation imaging.

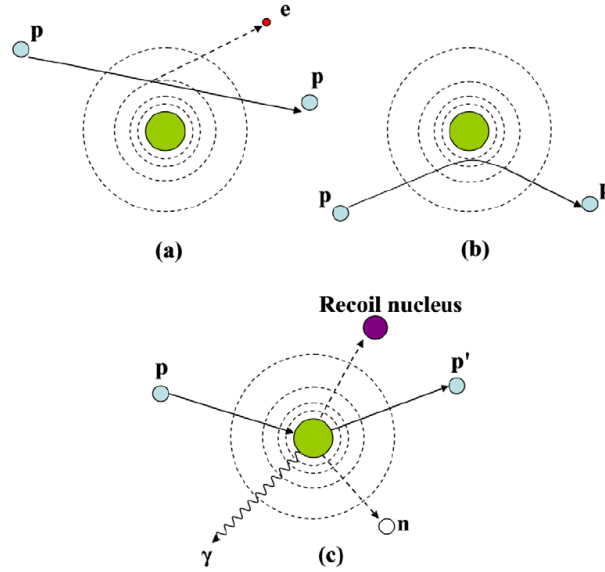


Figure 2.2: Diagram illustrating the interactions of proton: (a) energy loss due to inelastic Coulomb interaction, (b) a particle is deflected by a lossless elastic Coulomb interaction with the atomic nuclei, (c) a collision with a nucleus producing a recoil nucleus and various secondary particles due to non-elastic nuclear interaction (p: proton, e: electron, n:neutron, γ : gamma rays) [15].

2.2.2 Energy Loss and Energy Deposition

The rate of energy transfers per unit distance between the particle and absorbing material is given by the formula which is shown in equation 2.1 [15]:

$$-\frac{dE}{dx} = \rho 4\pi N_A r_e^2 m_e c^2 \frac{Z}{A} \frac{z^2}{\beta^2} \left[\ln \frac{2m_e c^2 \gamma^2 \beta^2}{I} - \beta^2 - \frac{\delta}{2} - \frac{C}{Z} \right], \quad (2.1)$$

where N_A is Avogadro's number, r_e is the electron radius, m_e is the mass of an electron, ρ is the density of the medium, z is the atomic number of the beam particle, $\beta=v/c$ is the speed of the particle relative to c and I is the mean excitation energy of the medium. This equation is known as the Bethe-Bloch or Bethe formula [16]. The C/Z ratio is important only for very low energy particles and also depends on

the atomic structure of the target material. As a result, this term can be ignored. Likewise the δ term is only significant for very-high-energy particles and can be also ignored for the proton and alpha particles that we consider as they are ultra-relativistic. Figure 2.3 shows a plotting of the Bethe formula with the discussed approximations for proton and alpha. Alpha has energy loss much greater than the proton.

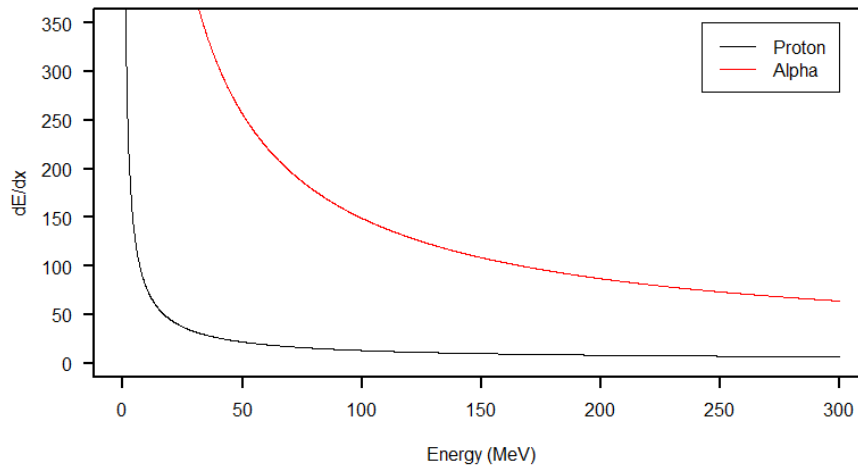


Figure 2.3: The rate of energy loss of protons and alphas as a function of energy following the Bethe formula with appropriate approximations.

The figure 2.3 shows that the rate of energy loss of an incident particle over a propagation distance due to charged particle interactions is proportional to the square of the particle charge and inversely proportional to the square of the particle velocity, *i.e.* faster incident particles have lower energy loss rates. As a result, the rate of energy loss increases as the particle slows down, reaching peak energy loss as it comes to a stop. Moreover, the deposited dose is therefore at a minimum at shallow penetration depths as the incident particle is at its highest velocity. This is what causes the aforementioned Bragg peak. Physically, this principle can be explained by understanding that a faster charged particle will pass by an atom quicker and is only subject to Coulomb force interaction for a short time. Conversely, a slower charged particle will pass slowly and interact for longer. Moreover, the tail following the initial sharp decay after the Bragg Peak, see figure 1.4, can be understood knowing that ions with higher atomic numbers have a larger interaction cross-section and direct nuclear interactions and fragmentation have increased probability of occurring. These secondary scattered particles result in further interaction processes over time causing energy depositions beyond the Bragg peak forming a fragmentation tail. However, the amplitude of the Bragg peak itself de-

depends on both the mass and range (velocity) of the incident particle. This is due to there being a constant energy deposition up until the penetration depth. The deeper the penetration depth, the higher percentage of total energy already deposited by the time the Bragg peak/stopping is induced.

Landau Distribution

The Bethe-Bloch equation 2.1 gives an average value of the energy loss of an individual particle. However, in reality the losses are random and, for a given case, the energy loss may be less or more than this averaged value. A more realistic probability distribution for this energy loss can be predicted by the Landau distribution [17]. This involves a universal function of a variable λ which can be described as:

$$f(\lambda) = \frac{1}{2\pi i} \int_{a-i\infty}^{a+i\infty} e^{lns+\lambda s} ds = \frac{1}{\pi} \int_0^{\infty} e^{-tln t - \lambda t} \sin(\pi t) dt. \quad (2.2)$$

In applying this integral to a physical situation, the loss of some energy Δ over a distance x , involves a scaling, ξ , and location parameter, Δ_0 , where

$$\lambda = \frac{\Delta - \Delta_0}{\xi}, \quad (2.3)$$

$$\xi = \frac{2\pi N_A r_e^2 Z z^2 m_e}{A \beta^2} \rho x, \quad (2.4)$$

and

$$\Delta_0 = \xi \left(\log\left(\frac{2m_e \beta^2 \xi \gamma^2}{I^2}\right) + 1 - \beta^2 - \gamma_e \right). \quad (2.5)$$

For a particle of charge, z , in a material with atomic weight, A , and atomic number, Z . ξ and other energies are in MeV and ρ is in g/cm^2 . I is the mean ionisation energy taken as $10Z$ eV, and γ_e is Euler's constant. The probability density function (PDF) of Δ can be written as:

$$P(\Delta) = \frac{1}{\xi} f\left(\frac{\Delta - \Delta_0}{\xi}\right). \quad (2.6)$$

In this regard, Δ_0 is similar to the Bethe-Bloch energy. It has no direct physical meaning but it is very close to the peak of the distribution. The form of the Landau equation is really due to statistics rather than physics. The energy loss is made of a very large number of energy losses on individual atoms. A particular energy loss can be made of individual energy losses in many different ways. The statistics of that leads to a differential equation, which can be solved using a Laplace transform and gives rise to the form shown in equation 2.2. The only physics modelling included is the probability of small energy losses, (δE) , which is proportional to $1/\delta E^2$.

Note that the form shown of the Landau distribution in equation 2.2 cannot be written down in an exactly calculable form. However, several numerical approximations exist, including that of Wilkinson - which was used to draw figure 2.4 [18]

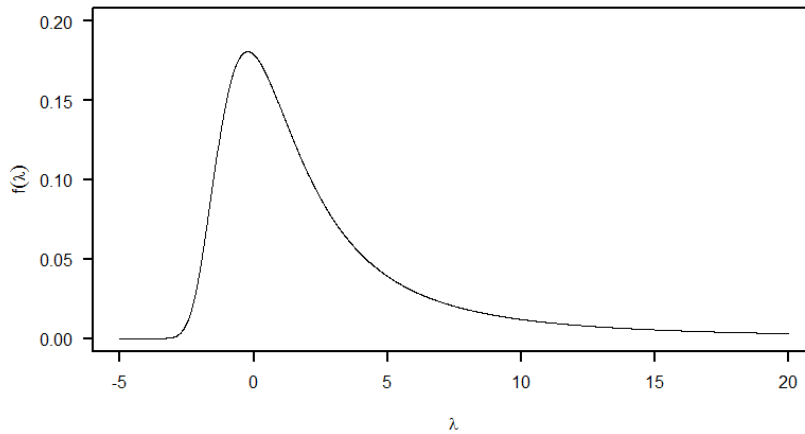


Figure 2.4: The Landau distribution as a function of λ .

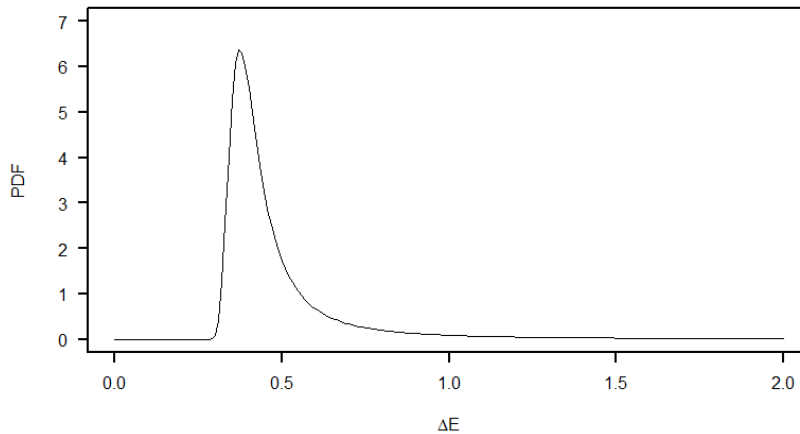


Figure 2.5: The probability density function of ΔE obtained from the Landau distribution that is for 80 MeV proton in 500 μm target.

Notably, figure 2.4 only shows the universal Landau function for one particular application. One may calculate ξ and Δ_0 and subsequently use them to map actual energy losses Δ to the universal parameter λ . An example of this is shown in the figure 2.5 for 80 MeV proton at the thickness of the target at 500 μm for which ξ is 0.028 and Δ_0 is 0.379. The Landau distribution is correctly normalised so that the PDF is always integrated to one. However, if higher moments do not exist, the $\int \lambda f(\lambda) d\lambda$ and $\int \lambda^2 f(\lambda) d\lambda$ do not converge. The integrals distribution does not

have a mean or a standard deviation. The scale factor size is proportional to the thickness x . The location parameter Δ_0 is, however, not exactly proportional to x . But in the cases we consider, this non-linearity does not give a significant effect.

2.2.3 Linear Energy Transfer (LET)

The International Commission on Radiation Units and Measurements (ICRU report no.85) defines the linear energy transfer (LET) as the average of the energy imparted in a unit length of the track of the particle. It can be written as:

$$LET = \frac{dE}{dx} \quad (2.7)$$

The energy loss by the particle, dE , for a given penetration distance, dx , is, however, not always the same as the energy gained by the medium. High energy particles can give nuclear reactions resulting in undetectable neutrinos and long lived nuclear products. Interaction processes may also produce photons which travel such a long distance from the site of the original interaction prior to absorption such that the energy is effectively lost. One must also consider the production of the secondary particles and subsequent scattering and further interactions. Should these losses be counted towards the total energy loss from the parent track or be considered a unique track in their own right. Due to the possibility of confusion, in the context of this thesis, dE and ‘energy loss’ refers explicitly to the energy lost by the particle. Any such reference to the deposited energy brings in a cutoff to define what is meant by ‘local’, and/or what energy of excited electron is considered as a delta ray (the Geant4 ‘production cut’). This is referred to as either the ‘unrestricted LET’ or ‘stopping power’ - shown in figure 2.6 for energy loss and energy deposition for an incident proton of different energies penetrating a water target.

This plot was produced by the author using Geant4 - described in more detail in chapter 3. At each step, the incoming and outgoing of the charged particle were used to give energy loss and the energy deposition from the built-in function in Geant4, called `GetTotalEnergyDeposit()`. They agree very well, especially in the Bragg peak which is the most important aspect for practical radiotherapy. At the low beam particle energy, there are fewer reactions that generate nuclear processes or lost photons.

The distance, as a denominator of the equation 2.7, is also ambiguous. We consider a particle travelling normally through a ‘target’ of thickness x . It is, however, important to note that the actual distance from entrance point to exit will be bigger because of scattering. The distance travelled will be larger again because of multiple scattering. Now, strictly the third definition of distance is the correct one because it is the actual distance that particles travel. However, it is impossible to measure. The start to the finish distance, the length along the chord, is sometimes used and this is known as the lineal energy transfer [19]. For simplicity, the

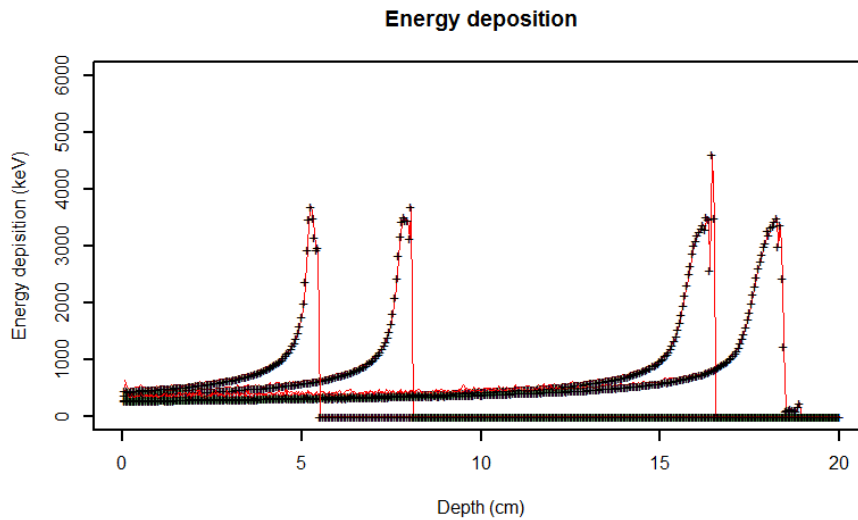


Figure 2.6: The energy loss as a function of depth for protons of energy 80, 100, 150 and 160 MeV. The red line displays the energy loss and the black crosses represent the energy deposition.

‘Depth’ depicted is the simple target thickness. Again the differences are small and insignificant.

This is shown in figure 2.7. The results shown were obtained from Geant4 simulation of 80 MeV proton travelling through a succession of 500 μm thick slices of a water target. The chord length was calculated from the entrance and exit points. The total length was provided by the Geant4 built-in function, called `GetStepLength()`. Both approaches of getting length are similar and close to the thickness of the target of 500 μm . The ratio of the length is close to 1 as it shown in figure 2.7.

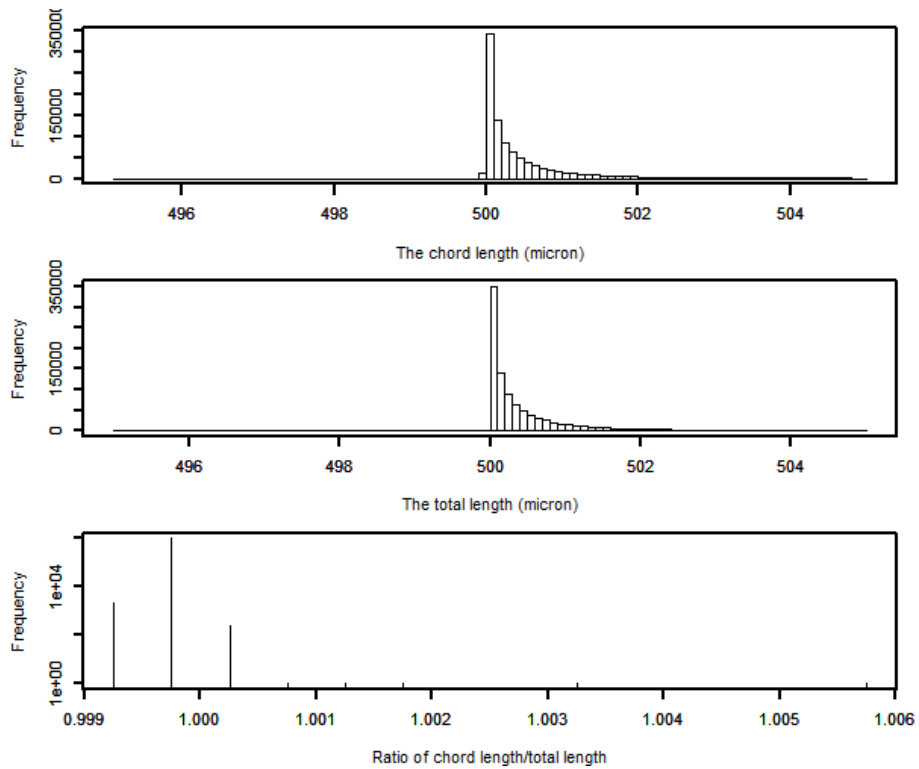


Figure 2.7: The plot shows the distance obtained from Geant4 simulation when using different methods, top: the chord length, middle: the total length and bottom: the ratio of the chord length and total length

LET_t and LET_d

There are two methods to calculate the LET, the so-called track-averaged LET (LET_t) and the dose, or energy, averaged LET (LET_d). LET_t is derived by averaging the energy deposited from a track of particle scored in a volume over a length that the particle propagates within that target. LET_d is obtained by averaging the track over equal dose or energy increments. The weighting factor of LET_d is from the individual energy deposition event. Figure 2.8 shows the concept of LET_t and LET_d calculation. These two definitions, and the way in which they are calculated, are further discussed in section 3.2.

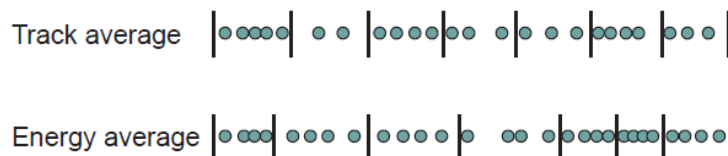


Figure 2.8: Calculation of track-average LET and dose-average LET [20]

2.2.4 Track structure

The stochastic pattern of interaction of radiation is called track structure. It is important for radiation biology as it is one of the factors that influence the biological outcome induced by ionising beam. Figure 2.9 shows the track structure of proton and alpha particles at energy of 1 MeV and 10 MeV obtained from the simulation in water material [21]. It can be noticed that even the particle at the same incident energy does not have the same energy distribution. Both of alphas produce denser interaction especially alpha that of 1 MeV. From this simulated result, it is challenging to understand the impact of pattern of the track on the living cells. The spatial distribution is suggested to define the density and complexity of the damage. The more complexity of the damage the more difficult to repair. So that the distribution of energy distribution would be related to the spatial distribution of damages. The modelling of radiation-induced damage to quantify the number DNA damage is based on this assumption.

It is still difficult to measure the cell reaction to radiation in molecular resolution. The experiments in nanodosimetry attempting to reveal the spatial distribution of energy distribution detected in gas enables the investigation of energy cluster of various charged particles [22, 23]. These experiments can then be scaled to represent water. Therefore, the study of track structure of charged particle is active research topic in both experiment and through simulation to determine the impact of the pattern on living target cells.

2.3 Radiation Biology

After irradiation, living cells may experience different interaction of radiation. In this section, DNA structure and type of radiation-induced DNA damage will be discussed as it is considered to be responsible for the survival of the cells.

2.3.1 DNA structure

DNA is formed by two strands of nucleic acids linked together with a hydrogen bond forming a helix structure with a diameter of approximately 2 nm. Each base has a specific base pair, i.e., Adenine(A) and Thymine(T), Cytosine(C) and Guanine(G). The repeating units of nucleotide, as shown in the figure 2.10, form into a DNA strand of double helix coil and then wrap around the histone protein to form a nucleosome. The sugar-phosphate group of the nucleosome is known as the DNA backbone. The backbone is considered as a susceptible part for DNA damage. Figure 2.11 is an illustration of DNA organisation when the nucleosome, a building block of DNA strand, are coiled tightly into a long DNA strand. The diameter of the chromatin fibre is approximately 30 nm. The long strand of chromatin is packed densely into a chromosome.

Basically, there are three main DNA forms which can be found in nature. The most typical form is called B-DNA. The differences between each form are struc-

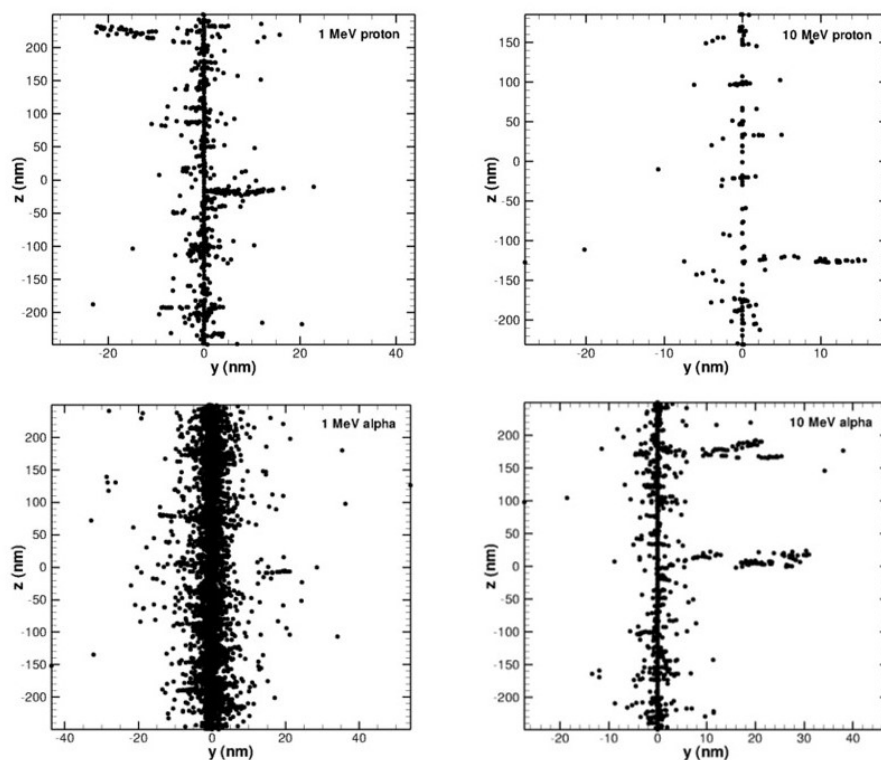


Figure 2.9: Track structure of proton and alpha particles taken from [21]

ture, angle between two strands. A comparison of each DNA form is shown in the table 2.1. Figure 2.12 also shows the illustration of DNA structure presenting in A-DNA, B-DNA and Z-DNA, respectively. In addition, the structural parameters of B-DNA conformation are shown in figure 2.13. These parameters were used in the modelling of DNA strand presenting in chapter 4.

In human cell nucleus, it has approximately 6 billions base pair (6 Gbps)[27]. The genetic information is stored in the combination of three bases called a triplet codon. The codon acts as a genetic code which can be transcribed to RNA for protein synthesis. For example, a RNA sequence of AUG and UAA represents a start codon and stop codon transcribed from DNA, respectively, of a replication process. Therefore, the alteration of this sequence of the codon would cause an erroneous message to be passed to the daughter cell. The genetic code carries essential information for cell proliferation and reproduction which is densely packed with protein inside the cell nucleus. Because DNA can control and regulate cell's behaviours including the transcription of genes to daughter cells, it is considered as a critical target in Radiobiology [28, 29, 30].

Ionising radiation can induce the DNA break when interacting with the DNA strand especially sugar-phosphate backbones. A single strand break refers to the situation which only one of the backbone is damaged. A single strand break can be

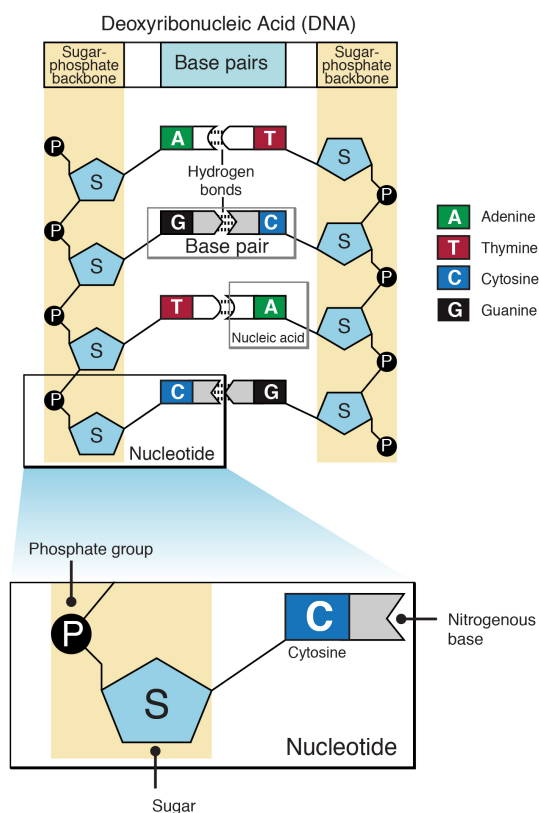


Figure 2.10: Nucleotide is the basic unit of DNA which compose of phosphate group, sugar and nitrogenous base. This also shows a scheme of base pairing of the double helix structure where two bases of, A:T or C:G, are linked together with hydrogen bond. [24]

repaired simultaneously by using the opposite strand as a template as each base fits to a specific base pair. However, there is still a chance of mutation arising from base alteration. The damage become substantial when the radiation triggers breaks on both strands of the DNA as it is more difficult to repair. The probability of inducing double strand break increases with the dose and the LET of the radiation. There is also evidence suggesting that cytotoxicity, ability to destroy the cell, arising from unjoined double strand breaks [31].

2.3.2 Direct and indirect effect of radiation

When the radiation passes through the medium, it can cause the ionisation by ejecting the electron in an atom. The interaction of ionising radiation can be categorised into two types when considering how the beam interacts with the living cells: direct ionisation and indirect ionisation.

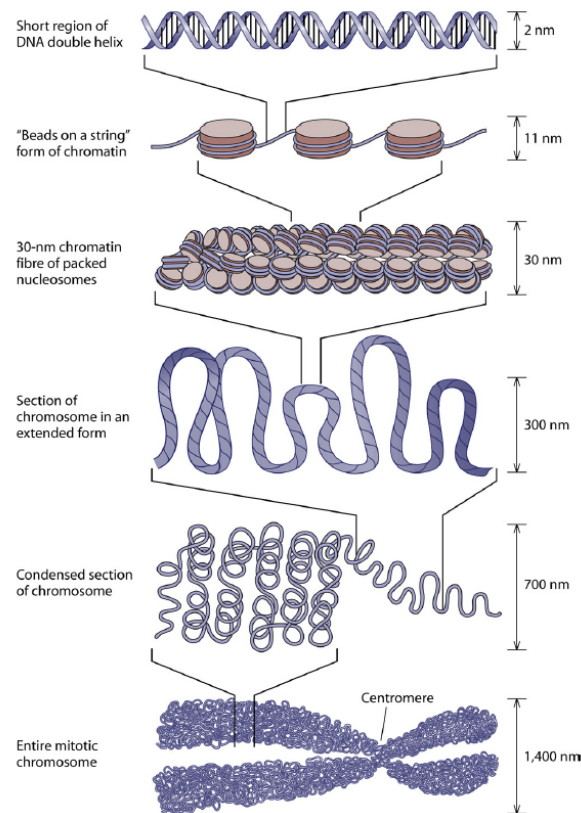


Figure 2.11: Structure of DNA [24]

For direct ionisation, the beam which has enough kinetic energy interacts directly with human tissue by causing chemical and biological damage to the genetic material. In other cases of indirect ionisation, a secondary electron can sometimes be produced when the energy imparted to the cell which mostly contains water. Then the free radical is produced and interacts with genetic material inside the cell leading to cell damage. Direct and indirect interaction on a DNA strand are depicted in the figure 2.14.

2.3.3 Relative Biological Effectiveness (RBE)

The definition of RBE is as simple as the ratio of the dose of radiation of interest and the reference radiation which produce the same biological effect. However, by this definition, RBE is complicated by its own as there are large variations of what is meant by 'biological effect'. To examine radiation-induced biological effect of a certain type of radiation, especially in the *in vitro* experiments, it should be performed and controlled ideally in the identical condition in order to get the meaningful results. Because conditions of such experiments can be varied from one study to another, due to differences in culture, experimental setup and radiation

Table 2.1: Comparison of A-DNA, B-DNA and Z-DNA conformation [25, 26]

Structural parameter	A-DNA	B-DNA	Z-DNA
Shape	Broadest	Intermediate	Narrowest
Direction of helix rotation	Right-handed	Right-handed	Left-handed
Distance between BP per turn of helix	0.23 nm	0.34 nm	0.38 nm
Tilt of base pairs from normal to helix axis	19°	1°	9°

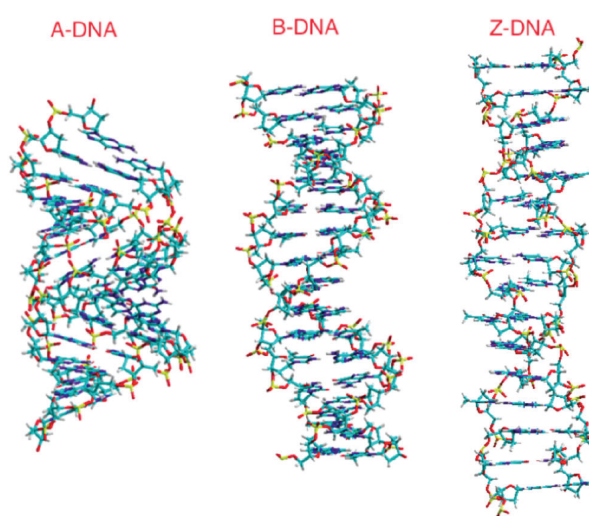


Figure 2.12: Structure of DNA in different conformation [26]

facility, the uncertainty of implementing the RBE as a universal term to compare between the studies is subject to considerable uncertainty.

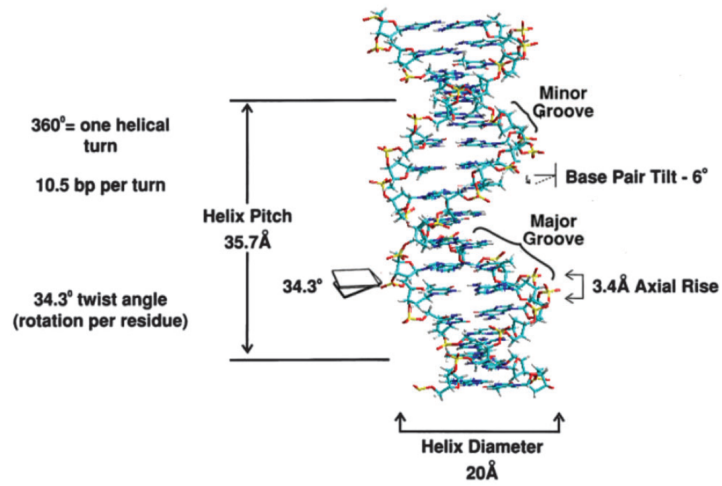


Figure 2.13: Structural parameters of B-DNA conformation [26]

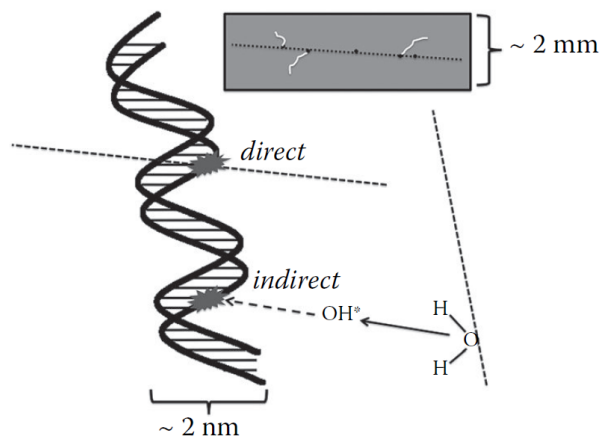


Figure 2.14: Direct and indirect damage to a DNA strand [32]

Chapter 3

Simulation of radiation quality using Geant4 code

This chapter describes methods of implementing the Geant4 Monte-Carlo simulation toolkit and performing the calculations used in this study.

3.1 Geant4 and Geant4-DNA code

Geant4 toolkit is written in the C++ programming language with object-oriented techniques. The purpose of this toolkit is initially for high energy physics experiments but it has been widely used for medical application for many years. The toolkit is organised into classes of various functions which can be invoked when needed. Different functions are designed for specific tasks used in the simulation which also include basic functions for handling geometry as a scoring target, tracking primary and secondary particles in order to obtain coordinates (x , y , z) of physical interaction and local energy deposition [1]. This work uses the Geant4 toolkit version 10.04, patch 2, which was released on 25 May 2018. There have been subsequent releases (the current version is 10.06) but they offer no relevant improvements for our purposes. The standard Geant4 was used for the simulation described in this chapter and Geant4-DNA was applied for the study in the following chapter.

Geant4 code is capable of implementing physical processes in the simulation including electromagnetic, hadronic and optical processes. A set of physics models is called a ‘physics list’ in Geant4. The QGSP_BIC_HP reference physics list was used particularly in this chapter, as it is recommended for the therapeutic range of proton energy in medical applications [33, 34]. The electromagnetic processes are managed with `G4EMStandardPhysics_option4`, implementing an algorithm based on the Bethe-Bloch energy loss formula for proton transportation, when the reference physics list is activated.

3.1.1 Geant4-DNA

Geant4-DNA is an extension of Geant4 toolkit for modelling the effect of radiation in the microscopic level especially on biological systems [35]. It includes physical and chemical models in order to simulate radiation-induced damage at cellular and subcellular level. The physics packages provided in Geant4-DNA extension have been validated with experimental data in water and against another toolkit [36, 37]. This extension enables event-by-event tracking of particles in sensitive volume down to low energies by modelling a series of steps of particle tracks. Figure 3.1 shows the difference between using the standard Geant4 model and the Geant4-DNA extension as a set of electromagnetic processes has incorporated in Geant4-DNA. This allows a tracking of low energy particles in liquid water. This Geant4-DNA is used for the simulation in Chapter 4.

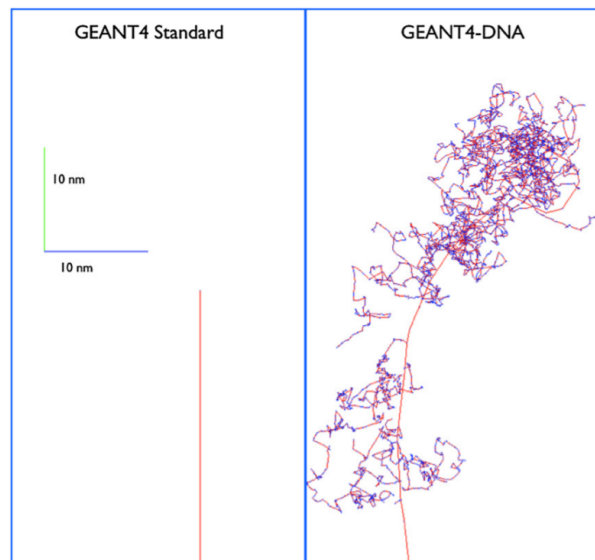


Figure 3.1: Standard Geant4 and Geant4-DNA extension simulation [4]

3.1.2 Basic setting in Geant4 simulation

In Geant4, there are three mandatory classes: `DetectorConstruction`, `PrimaryGeneratorAction` and `PhysicsList`. The `DetectorConstruction` class is for handling the dimensions and material of the geometry in the model. It allows users to create their own geometry to use in the simulation. In order to score or obtain information of physics processes and physical quantities including charge, momentum, energy deposition and particle fluence occurred in certain regions, the ‘sensitive’ areas have to be specified. This means that interactions or particles travelling outside this scoring area are not recorded.

In addition to setting up a geometry, the user should select an appropriate

physics package known as the `PhysicsList` depending on the purpose of the simulation as there are various physics models available in Geant4.

Finally, the `PrimaryGeneratorAction` class controls initial position and direction of the source, energy spectrum and angular distribution in the simulation.

In this study, different geometries, physics libraries, source positions and direction setup are implemented according to the purpose of the investigation. The setup of the simulation is given for each chapter.

3.2 Calculation of LET_t and LET_d in the simulation

The definition of LET is mentioned earlier in section 2.2.3 but, in this section, it will be presented in greater detail for the calculation in Geant4 simulation.

The total energy deposition, ε , is the energy imparted in a discrete step by a charged particle. The step length, l , is a length of a small step made by a charged particle as it traverses in the scoring volume. Both ε and l can be obtained by invoking the built-in functions in Geant4 called `GetTotalEnergyDeposit()` and `GetStepLength()`, respectively. Therefore, energy deposition per step, as a definition of LET, is equivalent to ε/l . Figure 3.2 shows the definition of step (i) and energy deposition ε in Geant4.

In calculating tracked average LET (LET_t), this can be expressed as:

$$LET_t = \sum_{i=1}^n \left(\frac{\varepsilon_i}{l_i} \right) \omega_{i,t} \quad (3.1)$$

Where i is the number of step, n is the total number of steps made by a track of charged particle and $\omega_{i,t}$ is the weighting factor, can be defined as:

$$\omega_{i,t} = \frac{l_i}{\sum_{i=1}^n l_i} \quad (3.2)$$

Therefore, the ratio of the total energy depositions and total track lengths by all particles can be written as:

$$LET_t = \sum_{i=1}^n \left(\frac{\varepsilon_i}{l_i} \right) \omega_{i,t} = \frac{\sum_{i=1}^n \left(\frac{\varepsilon_i}{l_i} \right) l_i}{\sum_{i=1}^n l_i} = \frac{\sum_{i=1}^n \varepsilon_i}{\sum_{i=1}^n l_i} \quad (3.3)$$

However, the relative dose distribution is used as the weighting factor for the calculation of dose average LET (LET_d) which can be expressed as:

$$LET_d = \sum_{i=1}^n \left(\frac{\varepsilon_i}{l_i} \right) \omega_{i,d} \quad (3.4)$$

Where $\omega_{i,d}$ is the dose weighting factor which can be described by:

$$\omega_{i,d} = \frac{D_i}{\sum_{i=1}^n D_i} = \frac{\epsilon_i/m}{\sum_{i=1}^n \epsilon_i/m} = \frac{\epsilon_i}{\sum_{i=1}^n \epsilon_i} \quad (3.5)$$

Where D_i is the dose deposited in i th event within the scoring volume of the mass m . The mass of sensitive volume is cancelled out in this case. Therefore, by substituting the dose weighting factor, equation 3.4 can be written as:

$$LET_d = \sum_{i=1}^n \left(\frac{\epsilon_i}{l_i} \right) \omega_{i,d} = \frac{\sum_{i=1}^n \left(\frac{\epsilon_i}{l_i} \right) \epsilon_i}{\sum_{i=1}^n \epsilon_i} = \frac{\sum_{i=1}^n \frac{\epsilon_i^2}{l_i}}{\sum_{i=1}^n \epsilon_i} \quad (3.6)$$

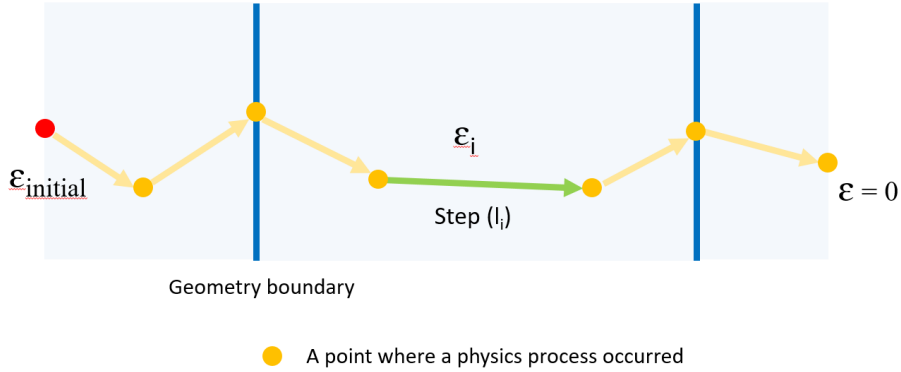


Figure 3.2: The illustration showing a series of steps of a particle track as it loses energy (ϵ_i) along the track. In Geant4, it allows event-by-event tracking from a starting point of initial energy ($\epsilon_{initial}$) until a particle stops as a kinetic energy of zero.

3.3 Distribution of energy deposition

A water box with a dimension of 20 cm×20 cm×20 cm was simulated in order to investigate energy deposition distributions. The radiation source was generated from the side of the target. There is a number of slides inside this water box for determining energy deposition as a function of depth. The number of the slides depend on the thickness of the slides. Different thicknesses of the slide were used: 10 μ m, 500 μ m, 1 mm and 2 mm. The scoring volume and the tracking processes are illustrated in figure 3.3. The number of repetition was set to 10,000 to make the simulation results achieve good statistics. All data were analysed by using the R programming code after the simulation. Figure 3.4 shows the distribution of LET_t

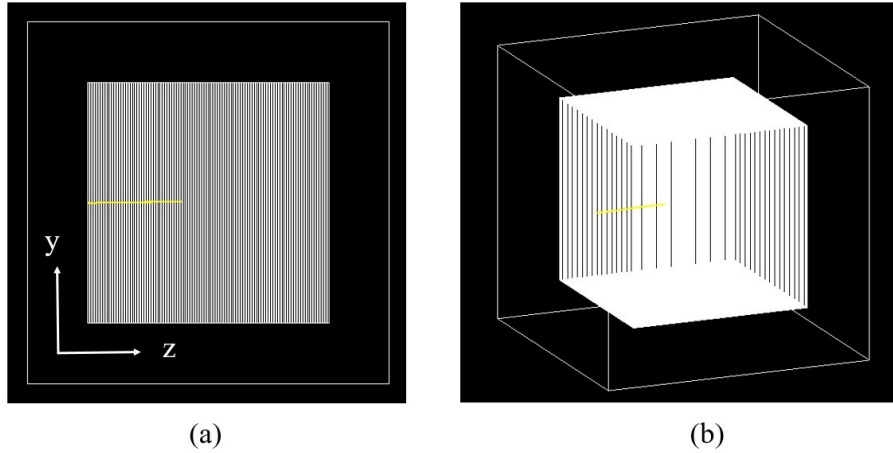


Figure 3.3: Geometry of energy deposition simulation: a box with a dimension of $20 \times 20 \times 20$ cm containing multiple slides for scoring energy deposited along a target depth. a) the side view on the y - z plane b) the view from another angle. Yellow line is a track of 100 MeV proton pointing towards z direction.

and LET_d of 80 MeV proton traversing through a slide thickness of $10 \mu\text{m}$ when considering at LET less than $10 \text{ keV}/\mu\text{m}$

Notice figure 3.4 c and d, the distribution of LET_t and LET_d have the same shape as the Landau distribution in the section 2.2.2. Geant4 as used here does not include the Landau distribution but it is the accumulation of small energy losses just as Landau proposed even though these all steps in the Geant4 tracking are not the same as the step travelled by the particle between individual atoms. The ratio of the two plots has been shown in the figure 3.5.

To investigate this, a simulation was run of protons travelling through thin layers of water. Figure 3.6 shows the energy deposited by 10,000 150 MeV protons in layers of water of thickness 0.5 mm, 1 mm and 2 mm. It can be seen that the location of the peak increases by a factor of 2 for each doubling of the thickness, but the spread of the peak increases by a smaller factor. This shows that the peak for small thicknesses is relatively broader than it is for large thicknesses. This is important because the shape of the histogram related to calculated LET_d values. The narrower the peak the lower the LET_d that is shown in equation 3.9.

Figure 3.7 shows the LET_t and LET_d obtained from the first 15 mm of the target, plotted against depth. The LET values increase slowly with depth due to the slowing down of the protons. The LET_d values are always bigger than the LET_t values. For the thickest slices (2mm) this difference is small, it increases for the thinner (1 mm) and thinnest (0.5 mm) slices.

The dependence on LET_d on track step size has been noted by Guan et al [38], although they regard it as 'erroneous'. In fact it is an inevitable feature of the definition of the quantity.

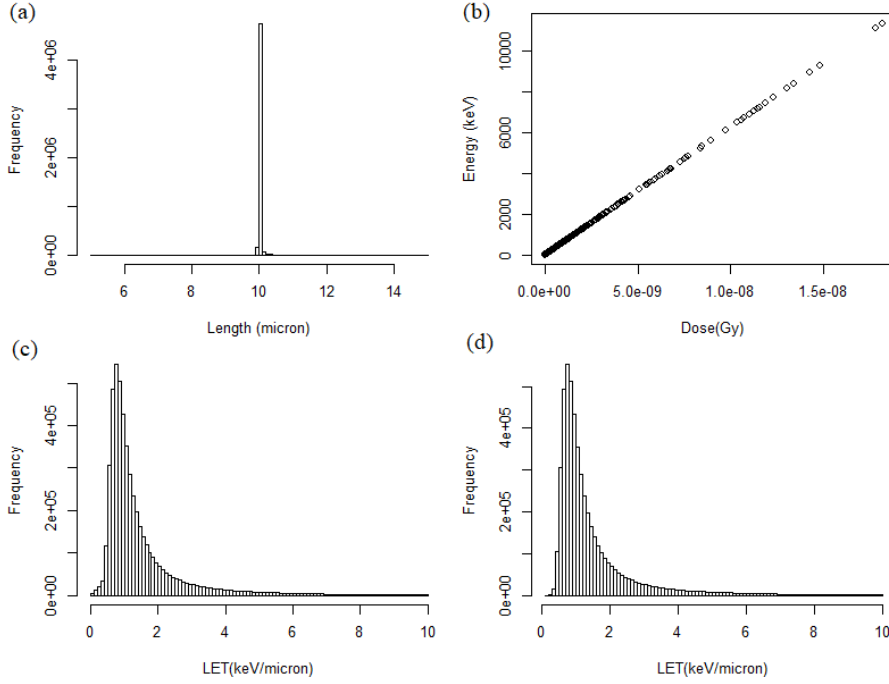


Figure 3.4: The plot of 80 MeV proton shows: a) histogram of a total length made by a particle track in the small slide of the volume b) the relationship between energy and dose deposited in the target c) the distribution of LET_t d) the distribution of LET_d

3.3.1 LET_d and stepping distance

The track average of the dE/dx squared is $\frac{\sum_{i=1}^n \frac{\epsilon_i^2}{l_i^2} l_i}{\sum_{i=1}^n \frac{\epsilon_i^2}{l_i}}$ which is $\frac{\sum_{i=1}^n \frac{\epsilon_i^2}{l_i}}{\sum_{i=1}^n l_i}$ which in turn is $LET_d \times LET_t$. So when looking at the energy distribution in figure 3.4c, the standard deviation

$$\sigma^2 = \left\langle \left(\frac{dE}{dx} \right)^2 \right\rangle - \left\langle \frac{dE}{dx} \right\rangle^2 \quad (3.7)$$

is given by:

$$\langle LET_t \rangle \langle LET_d \rangle - \langle LET_t \rangle^2 \quad (3.8)$$

which gives a useful expression for the difference for the LET_t and LET_d

$$\langle LET_d \rangle - \langle LET_t \rangle = \frac{\sigma^2}{\langle LET_t \rangle} \quad (3.9)$$

This shows that the LET_d is always greater. If one considers increasing the thickness of the target, according to the central limit theorem, the standard deviation increases by the square root of the thickness: as a number of sample n increases the spread increases like the \sqrt{n} so the proportional spread falls like $1/\sqrt{n}$. This

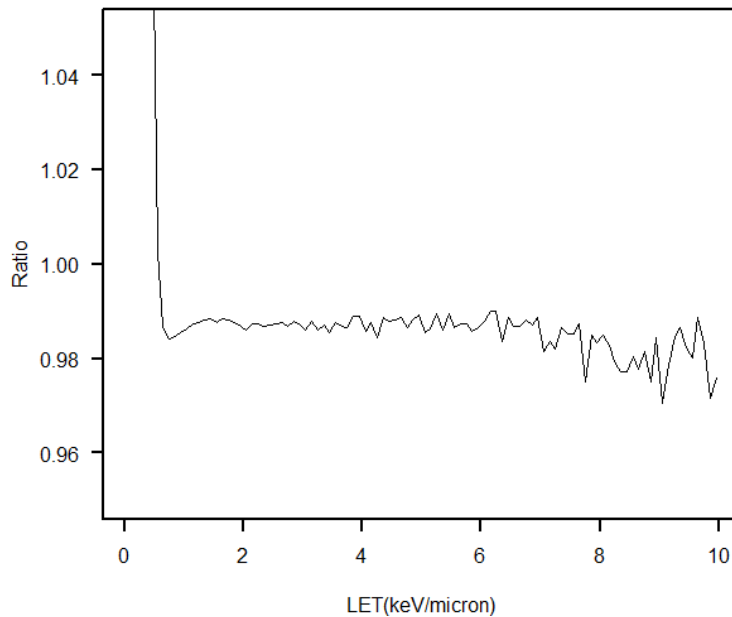


Figure 3.5: The ratio of the plots of the distribution of LET_t and the distribution of LET_d shown in figure 3.4

means that the difference between LET_t and LET_d can be large for a thin target but for a thick target the two are very similar.

So, it is very important to notice that the LET_d depends on the thickness of the sample considered whereas the LET_t does not. Any quoted LET_d value should give details of thickness of the target or equivalent length scale. Figure 3.8, LET_t and LET_d of protons at 80 MeV, 100 MeV and 150 MeV are plotted as a function of depth to investigate the impact of a target thickness on LET. Different colours represent different thickness of slices in the target which are shown in: blue 0.5 mm, green 1 mm and red 2 mm. The LET_t shows a good agreement between the different target thickness whereas LET_d obviously scatter in the plateau region.

3.4 LET simulation in small target

A box made of water with a dimension of $10 \times 10 \times 10 \mu\text{m}$ was used in order to determine LET in a cell-size target. The size of the target corresponds to a distance of a particle crossing the cell nucleus and cytoplasm. The primary particles were generated at the centre of the side of the target. The position, step length and energy deposited by a primary particle within the target were scored. There were 10,000 repetitions for each of energy of the primary particle. Then the averaged LET was calculated by using equation 3.3 and 3.6 for LET_t and LET_d , respectively. Figure 3.9 shows the LET_t as a function of initial energy of primary particles. Closed

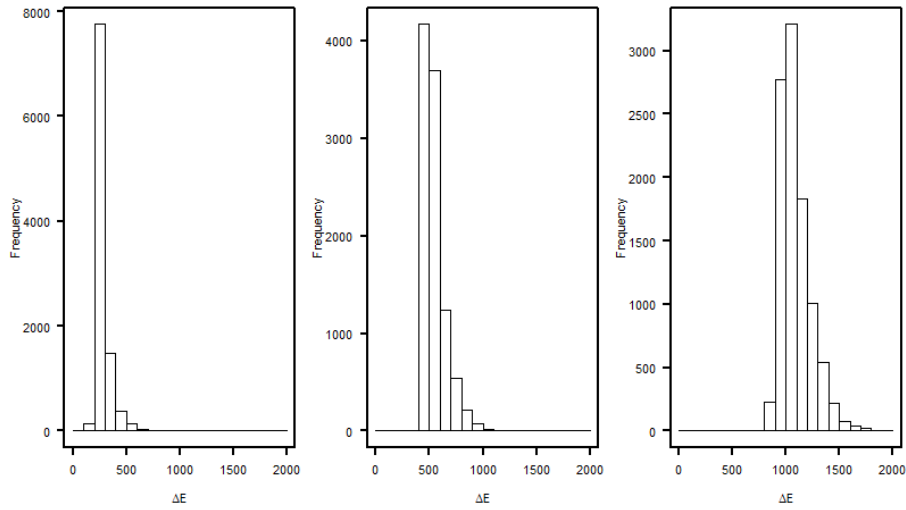


Figure 3.6: Energy deposition by simulated 150 MeV protons in a slice of water of thickness 0.5 mm, 1 mm and 2 mm

symbols are the results obtained in this work and open symbols are from other studies. There is generally good agreement, except that the LET_t of alpha particle of energy below 20 MeV/u shows a significant difference against other works. This is due to a difference in the physics list used.

To obtain a dose given by a track of particle, the amount of energy deposited within the target is divided with the mass of the target which is shown in figure 3.10. The deviation of proton and alpha particles, at above 10 keV/ μ m, from the calculated dose can be noticed. For very low energy particle, the distance travelled inside a target is longer than a target thickness due to straggling. The dose per primary particle (mGy) is plotted as a function of LET_t . This number is used to calculate a number of tracks required for a certain dose in the cell model in the next chapter. The straight line in the plot is the number predicted by the calculation.

3.5 Why the investigation of LET is interesting and important

Basically, delivering charged particle radiation to treat cancer does not just define by the dose, or even the dose multiply by a factor of RBE. It is generally accepted that the effectiveness of a dose depends on the LET [5, 29]. We have learnt that LET plays an important role in radiobiological outcome. It also suggests big dynamic variation in LET at the Bragg peak and the distal end of the particle tracks. This variation could have significant effect in damaging the cells. Hence, we should take LET into account properly in the treatment planning.

People sometimes ask whether one should use the LET_t or LET_d [39]. As

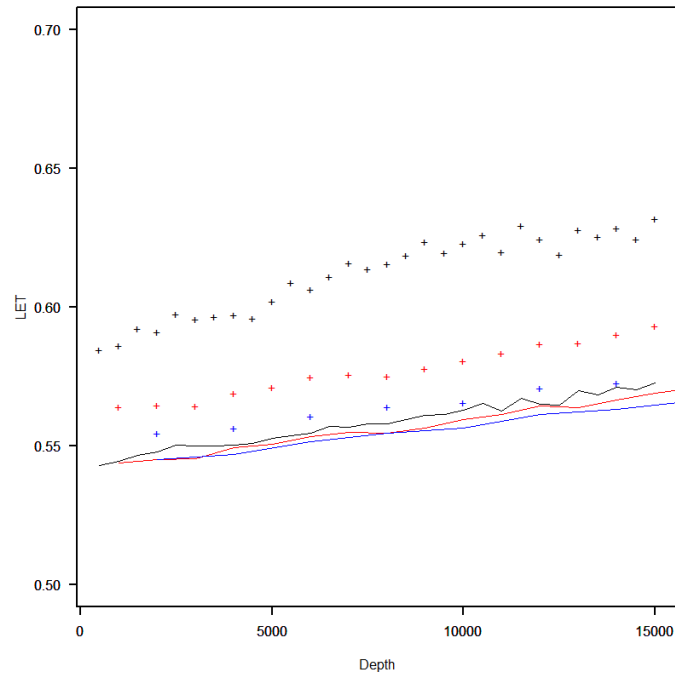


Figure 3.7: LET_t (lines) and LET_d (crosses) as a function of depth from Geant4 simulations of 150 MeV protons travelling through water in slices of 0.5 mm (black), 1 mm (red) and 2 mm (blue)

shown in figure 3.7 a different length scale gives a variation at the 10% level in the LET_d and that is significant. If the target is smaller than 0.5 mm, the difference is going to be substantial effect. Conversely, if one could establish what the appropriate LET_d is that would contain useful information of the size of the effective target. The analysis in section 3.3 also shows that this is an incomplete question. One should be asking whether one should use the LET_t or LET_d , and if the latter then what size of target should be used to calculate it.

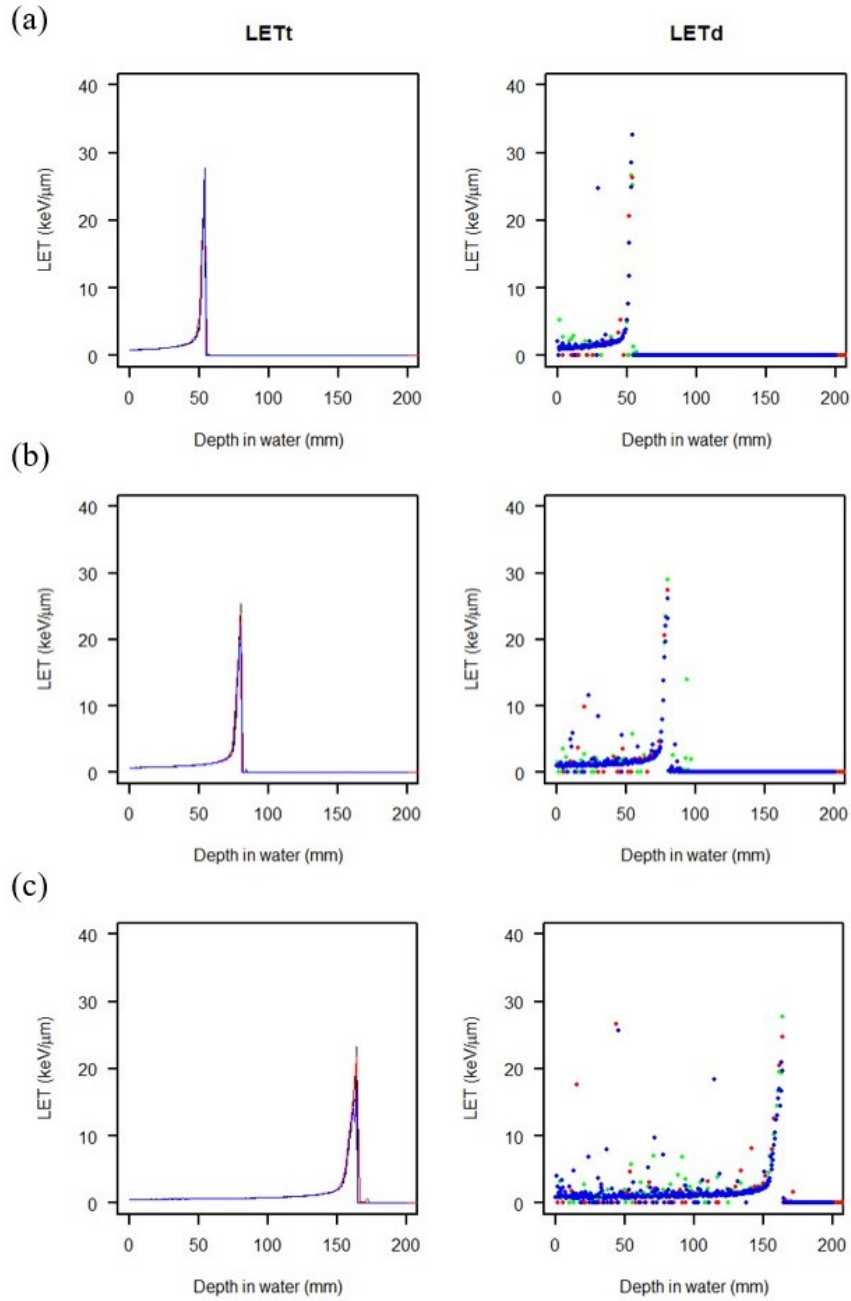


Figure 3.8: LET_t and LET_d of proton at a) 80 MeV, b) 100 MeV and c) 150 MeV as a function of depth. Different colours represent the slide thickness of the target of red: 2 mm, green: 1 mm and blue: 0.5 mm

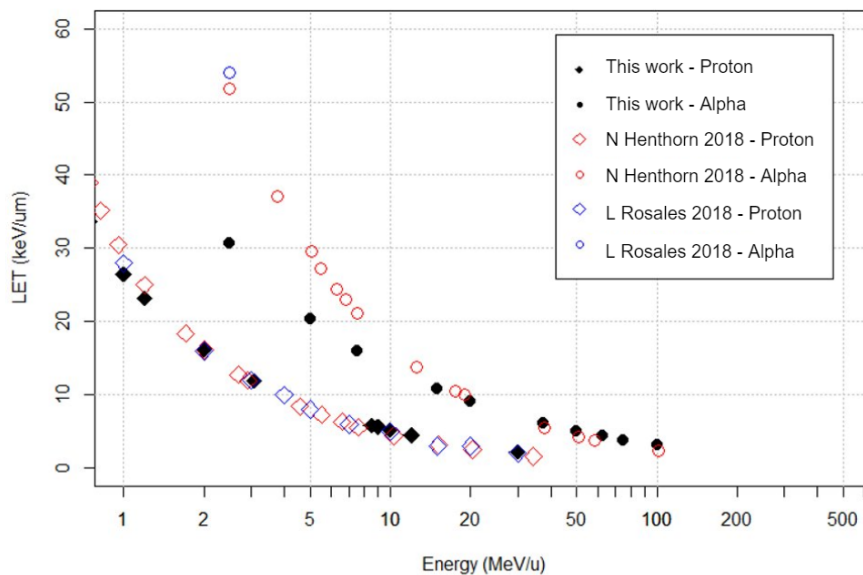


Figure 3.9: The averaged LET_t in a $10 \mu\text{m}$ target

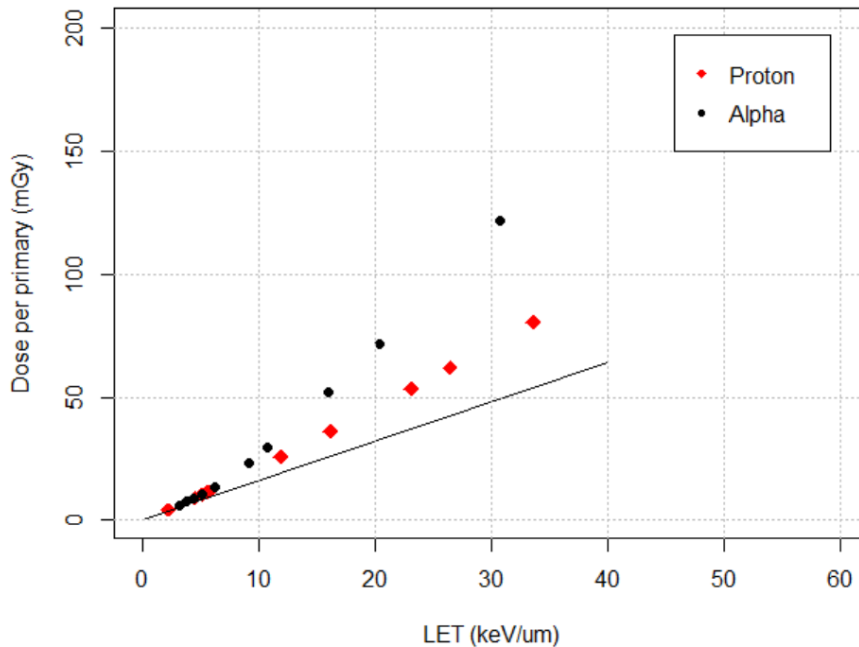


Figure 3.10: Dose of a primary proton and alpha as a function of LET_t ($\text{keV}/\mu\text{m}$). The straight line is the calculated dose

Chapter 4

Simulation of direct radiation-induced DNA damage

In this chapter, a model of DNA molecule is used in order to obtain the spatial distribution of energy deposition in the DNA structural model representing radiation-induced cellular damage.

It has been reported in the literature that the track structure of radiation and the organisation of chromatin fibre, the structure of DNA molecules and histone protein, are responsible for the implication on the biological effect [40]. This makes the radiobiological model important for determining this effect by incorporating structural features of a DNA molecule with the spatial distribution of the particle tracks. In this study, Geant4-DNA code with a detailed DNA structure was used to quantify the number of DNA breaks for proton and alpha particles at various incident energies.

4.1 Orientation of DNA model

The DNA model used in this study was based on the detailed geometry described in the publication by M Santos et al [41] which enables the determination of DNA damage at microscopic level. This model represents a fibroblast cell nucleus with the dimension of 23.64, 17.04 and 3 μm on x,y and z axis, respectively. The geometry consists of five compaction levels starting from a basic unit of DNA molecule to a chromosome: DNA double helix, nucleosomes, chromatin fibres, chromatin fibre loops, chromosome territories.

The DNA molecule was in a B-DNA arrangement, type of DNA forms are previously described in section 2.3.1, containing 200 amino bases on each strand and the backbone region. A sphere with a diameter of 0.96 nm was used to represent the DNA bases. The DNA strands wrap around a cylinder representing a histone protein molecule with a radius of 3.25 nm and length of 2.85 nm to form a nucleosome as shown in figure 4.1. There are 90 nucleosomes on each chromatin fibre. In the cell nucleus, there were 46 boxes equivalent to the number of chromosomes in

a human cell. This cell nucleus contains 332,500 pieces of chromosome fibre and 29,925,000 nucleosomes. Therefore, the number of base pairs is approximately 6×10^9 base pairs (6 Gbps) in total. The structure of chromosome territories is illustrated in figure 4.2. The cell nucleus was then placed in a water box with a dimension of $26 \mu\text{m} \times 20 \mu\text{m} \times 5 \mu\text{m}$ representing cytoplasm and the extracellular environment.

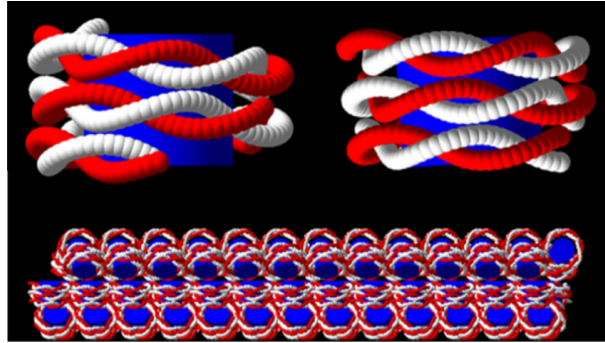


Figure 4.1: Organisation of DNA model in the cell nucleus target: top: nucleosome (blue: histone protein core, red and white: DNA double helix containing backbone and amino bases) bottom: chromatin fibre formed with nucleosome as basic unit of DNA structure [41]

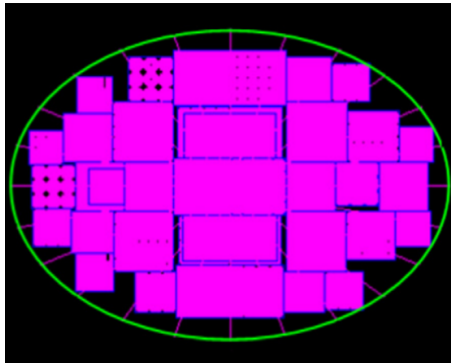


Figure 4.2: The chromosomes territories of the fibroblast cell nucleus model [41]

4.2 Simulation of physical interactions

The simulation was performed using the default Geant4-DNA physics package in order to quantify the number of DNA breaks. The DNA geometry as described in the previous section was filled with water. Even though the DNA geometry is composed of various sensitive regions, defined in the simulation, the material and the cross section data used in this work is defined as water. It is important to note

that, in most cases, the simulation of radiation-induced damage of biomolecule uses water as a material of the target because it is the major component of human cells. In addition, interaction cross section calculation of water is simpler than that of biocompounds. The Geant4-DNA physics package available in version 10.2 is derived from the cross section of water only.

The output from the Geant4-DNA simulation was saved into a separate text file which was further analysed with R programming code. The file contains the information of the energy deposition events, from a track of incident particle, located in the scoring volumes: sugar-phosphate group representing the backbone of the DNA strand and the base molecules. Every interaction occurred in the defined region was registered to strand 1 and strand 2 of the DNA molecule for DNA damage calculation. These information also include the type of interaction including excitation, ionisation and type of particle. The minimum energy deposits considered as capable of inducing DNA damage is 7 eV, 8 eV, 8.22 eV, 10.79 eV and 17.5 eV. For mono-energetic protons, the simulations were performed at the energy of 0.8 MeV, 1 MeV, 2 MeV, 4 MeV, 5 MeV, 10 MeV and 20 MeV. For simulations for alpha particles the initial energy were chosen at 2 MeV/u, 4 MeV/u, 10 MeV/u, and 20 MeV/u. For each primary particle energy, it was repeated for 1000 tracks. Table 4.1 shows the data entries of 1 MeV proton obtained from Geant4-DNA. First column, TrackID, represents a number of particle track starting from 0. A single track of particle can deposit energy in many steps producing many entries of the same trackID. Second column, particle, is the type of particle where 20 is proton and 10 is electron. Then the type of interaction or process is recorded according to the type of particle: 22 is proton ionisation and 12 is electron ionisation. The energy deposition (Edep) is recorded in keV and finally the position of x,y,z are in micrometer.

Table 4.1: An example of an output file of 1 MeV proton obtained from Geant4-DNA

TrackID	Particle	Process	Edep	Strand	x	y	z
0	20	22	13.39	1	8022.86	3776.57	-204.775
0	20	22	10.79	1	8023.13	3776.48	-187.753
0	20	22	10.79	1	8023.14	3776.48	-187.514
0	20	22	16.05	1	8025.93	3775.96	-38.6051
0	10	12	13.39	1	8039.39	3781.78	1069.6
0	10	12	10.79	1	8039.46	3781.83	1069.54
0	10	12	10.79	1	8049.14	3786.9	1065.67

To obtain a physical interaction on the DNA target, the particle was generated from the source placed above the cell nucleus and delivered to the direction parallel to the z axis as indicated by red arrows in the figure 4.3. In the study by P Pater et al.[42], the effect of the angle of the source relative to the DNA target is inves-

tigated and shows only a small variation of double strand break at very low angle. Therefore, in this study, the source is pointing parallel to the z direction only.

The dimension of cell nucleus model is illustrated in figure 4.3. The positions of the individual source were generated randomly to cover the area of the centre of the cell target, similar to what was done in other studies [12, 43]. This ensures that the target was irradiated uniformly avoiding the edge of the target. Figure 4.4 shows the example of the positions of 2 MeV and 5 MeV protons for each track generated and spread within the cell nucleus relative to the dimension of the nucleus on the x-y plane.

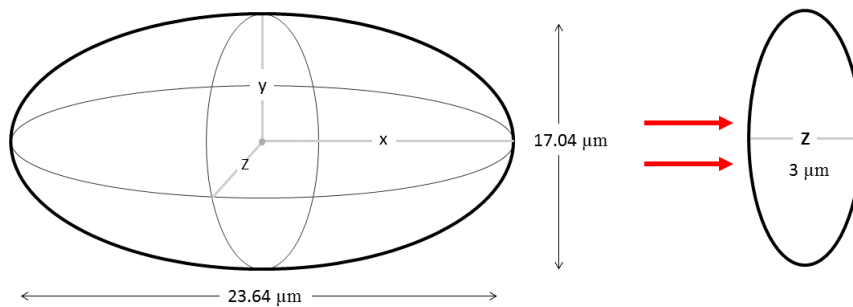


Figure 4.3: Dimension of cell nucleus in the cell model. Red arrows represent the direction of the beam from the top view.

4.3 Production of clusters of DNA breaks

The details of the physical interactions that may induce radiation damage to the biological cell is still an active research topic due to the lack of complete and accurate data on the physical interaction causing direct DNA damage [cite]. Basically, ionisation and excitation of the radiation arising on the DNA strand can lead to DNA damage. Processes of ionisation on the DNA hydration shell are generally considered as a direct DNA damage: a charge transfer process and a dissociative attachment which can affect the DNA structure. They can also be indirect damage due to the production of chemical radicals, but they are not considered in this study.

Therefore, in the mechanistic modelling, the assumption is made based on the amount of energy deposited on the DNA strand in order to predict biological response to the radiation. In this work, the number of direct single strand breaks of the early damage is calculated by the energy deposition inside a sensitive volume of the DNA model, especially where a sugar-phosphate group or DNA backbone is defined.

In the simulation of DNA damage, the definition of DNA break and classification of DNA damage complexity, known as cluster complexity, are varied from one study to another. Basically, a single DNA break (SSB) is induced when the

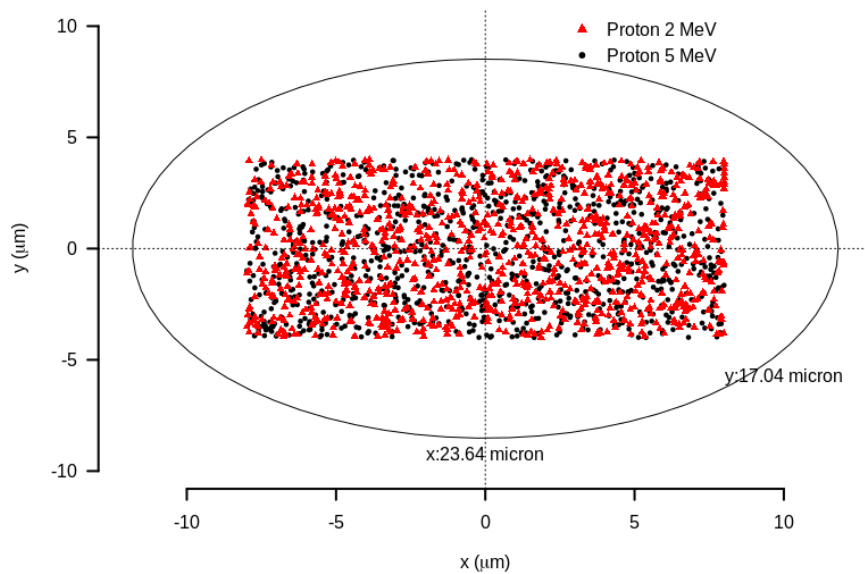


Figure 4.4: Positions of individual proton relative to cell nucleus dimension on xy plane

deposited energy from exciting or ionising interaction reaches above the defined energy threshold. The complexity of the damage inducing chromosome aberration is considered when there are at least two SSBs in close proximity. The detail on DNA cluster complexity and the calculation of DNA break yield is given in the section [4.3.2](#).

4.3.1 Algorithm for identifying energy cluster

After scoring energy deposited within the DNA backbone region of the DNA model, the coordinates (x,y,z) of excitation and ionisation events, energy deposit and strand ID of DNA (strand 1 and strand 2) were analysed in a separate programme.

A clustering algorithm, namely Density-based spatial clustering of applications with noise (DBSCAN), was used to analyse the number of DNA breaks induced by the ionising beam on the cell model. This algorithm is commonly used in data science including machine learning [44]. The principle of DBSCAN is to group numbers of point that are close together based on a specified distance and a minimum number of points required to form a cluster. Analysis in this way saves the running time in Geant4 as the DNA model contains billions of units of interest for DNA damage determination.

There are 2 input parameters required for DBSCAN: epsilon (ϵ) and mini-

mum points (minPoints). Eps is a radial distance between each point to be considered as part of a group or cluster. The algorithm starts with a point that has not been visited. Then, if there is a neighbour point which is close enough to a starting point within a distance of eps, they are grouped together in the same cluster. minPoints is the minimum number of neighbour points in the cluster. Once, the starting point and the neighbour points are registered to this cluster, these points are marked as visited. The algorithm then repeats for all points in the dataset. The point that is not included in the cluster is marked as a noise or outlier by DBSCAN. By changing the eps value, the number and size of the cluster would also change significantly. Small separate clusters can be formed into a single complex cluster as the distance of eps increases. So the optimal distance should be investigated when using this algorithm to investigate the cluster of DNA damage. The possible scenario is given in figure 4.5 which illustrates the impact of distance as a setting parameter in DBSCAN. In figure 4.5 (a), the spatial distribution of interaction within the region of interest and figure 4.5 (b) is when a certain eps is applied to these events. There are three small clusters obtained in this scenario including two clusters of two points and one cluster with four points. However, if the eps increases, it gives two clusters and one of them becomes a complex cluster with many interactions.

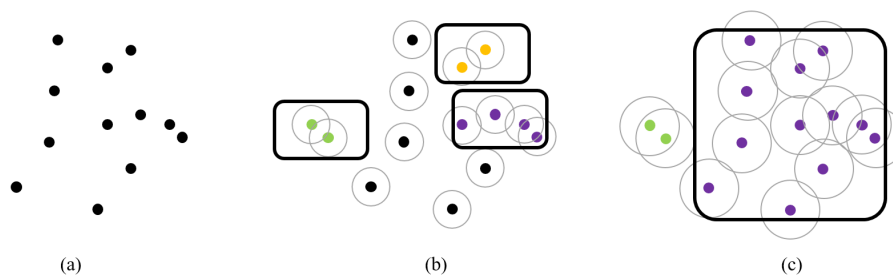


Figure 4.5: Illustration of spatial distribution of interaction. b) using a small distance there are three separate clusters c) the cluster becomes a single cluster with high complexity when adjusting the radial distance in DBSCAN algorithm.

When applying the DBSCAN algorithm for determining a type of damage, the eps is referred to the distance between DNA breaks and is usually defined as 10 base pairs apart [45]. Because DNA geometry use in this study contains a sphere of base pairs with a diameter of 0.96 nm, the length of 10 base pairs is then approximately 10 nm. Therefore, the eps was defined as 10 nm in this study. For minPoints, it was set to 2 as it needs at least two simple breaks to form a cluster.

In addition to the distance between DNA breaks, the threshold energy used as a production of DNA damage is also an important input parameter. An example is given in the figure 4.6. The three dimensional plot of interactions occurring within the backbone area from a single track of 1 MeV proton is shown. When applying the different energy threshold: 7 eV, 10.79 eV and 17.5 eV, the number of cluster

changes accordingly.

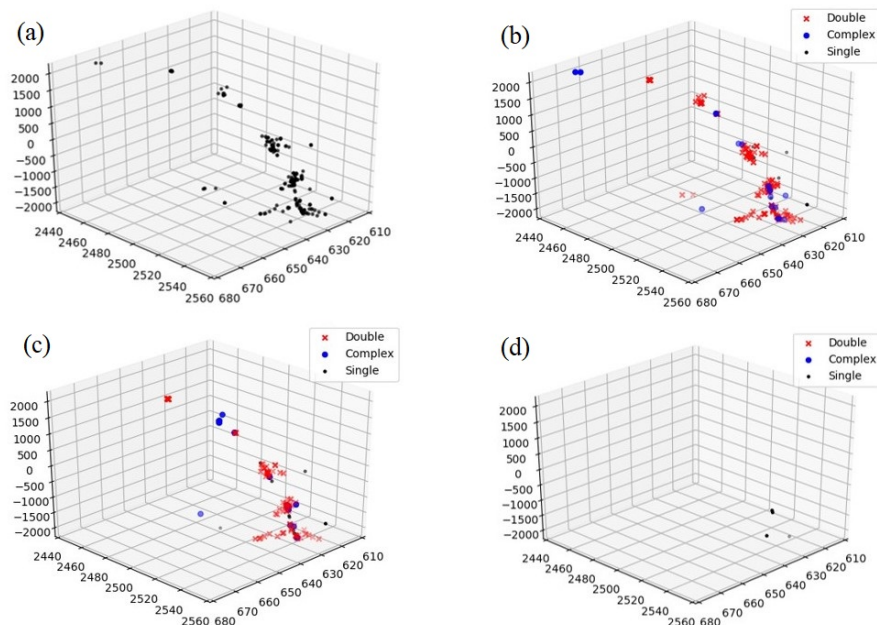


Figure 4.6: Example of varying the energy threshold in DBSCAN algorithm. (a) the spatial distribution of excitation and ionisation induced by a track of 1 MeV proton for all interaction. In order to investigate the optimal energy threshold for calculating a number of DNA break the minimum energy is varied to: (b) 7 eV, (c) 10.79 eV and (d) 17.5 eV

4.3.2 Calculation of DNA break yield

In this study, DNA breaks were classified into three types: simple single strand break (SSB), complex single strand breaks (CSB) and double strand breaks (DSB). When only one or two breaks occur on the same strand this is counted as a simple single strand break. However, if the cluster has more than 2 breaks in the same strand this produces a complex single strand break. When the situation that at least 2 breaks happen on the opposite strands, this is classified as double strand breaks. Figure 4.7 illustrates the classification of DNA break complexity.

Variations may arise when determining the DNA break yield as there are numbers of inputs parameters including energy threshold to be considered in producing DNA breaks, the critical distance between the interaction because the explicit length of double strand breaks is still an active research topic. The distance between two SSBs of 10 base pairs, used in this study is taken from the literature, based on the finding in a cell experiment [45].

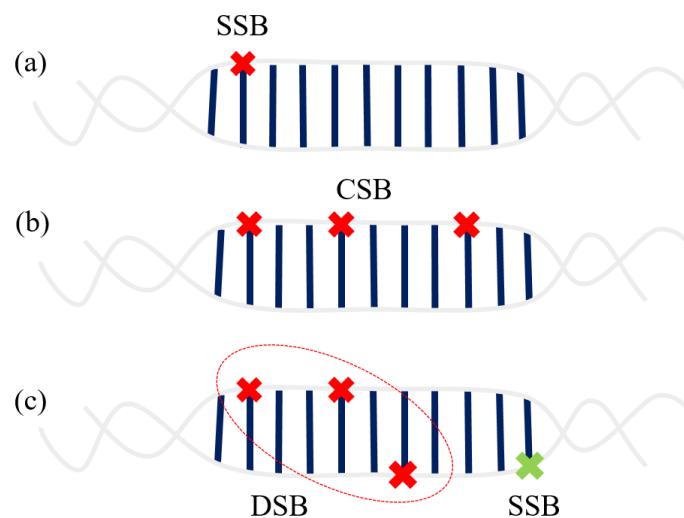


Figure 4.7: Illustration of DNA strand break definition: a) simple strand break (SSB), b) complex single strand break (CSB), and c) double strand breaks (DSB)

4.3.3 The optimal parameters for DBSCAN for determining energy cluster

It has been previously discussed that there is a variation of the number of SSB and DSB depending on the selection of the distance between two breaks and the minimum energy considered causing DNA break[46]. In this study, these parameters were varied in order to determine the difference on the SSB and DSB yields. However, the study investigating the arrangement of DNA model suggests that the yield of DNA break is not influenced by the structure of DNA model [47]. The list of energy threshold of DNA breaks used in the studies with Geant4 code is shown in the table 4.2.

4.4 Results and model validation

Figure 4.8 shows the average dose in the cell nucleus target given by a track of a particle as a function of the primary particle. It is obvious that the particle at low energy gives higher dose. In the figure 4.9, number of primary tracks required to the accumulate a dose of 1 Gy is given. This number of tracks is used as a reference for the calculation of DNA breaks.

The figure 4.10 displays the number of SSB, CSB and DSB of proton and alpha particles in the top and bottom row, respectively. The number of DNA break was calculated by using five different energies threshold at 7 eV, 8 eV, 8.22 eV, 10.79 eV and 17.5 eV as indicated in different colours. These minimum energies have been used in other studies as summarised in the table 4.2 . The number of DNA

Table 4.2: Energy threshold from other studies on the DNA model

Energy threshold	Refer to	Author
7 eV	lower than electronic excitation threshold of liquid water	B. Lee 2019 [48]
8 eV		M. Santos 2013 [41] L. Rosales 2018 [49]
8.22 eV	first excitation energy level of liquid water in Geant4 model	
10.79 eV	the lowest possible ionisation potential of liquid water	P. Pater 2016 [42]
17.5 eV		S. Meyland 2017 [12] N. Tang 2019 [43]

break is significantly dependent on the minimum energy defined in the clustering algorithm. The lower the energy threshold the more the number of DNA cluster can be found. However, for high energy particle it gives smaller number of DSB break and shows small variation between energy threshold compared to low energy particle.

Figure 4.11 shows the number of DNA breaks found from 200 simulated tracks where the energy deposits are presented to the DBSCAN algorithm grouped in different ways. First, each of the 200 tracks was presented on its own. Then tracks were taken in pairs, with 100 track pairs considered. This was followed by 50 sets of 4, then 40 sets of 5, and so on until finally a single ‘event’ of 200 tracks was analysed.

It can be seen that the variation in the number of strand breaks predicted is small. This remains true for different cutoff energies used, and for different proton energies, as shown. Figure 4.11 from our simulation shows no variation of the number of DNA breaks which the way in which the tracks are combined. Such combination represents the way in which different tracks are treated separately altogether.

The reason to look for such variation is that it could arise from different fractionation treatments if clustering between tracks is important. If two tracks are delivered in different fractions their effect simply adds, assuming cell repair times are shorter than the time between fractions. If they are delivered in the same fraction this is effectively simultaneous, and if the tracks are close the number of clusters can be different from the sum of those from the two tracks. It may be greater (if noise hits from different tracks combine to give a cluster) or lesser (if two separate clusters overlap and merge to form one big cluster).

The fact that no such variation is seen implies that, if the efficacy of a dose is

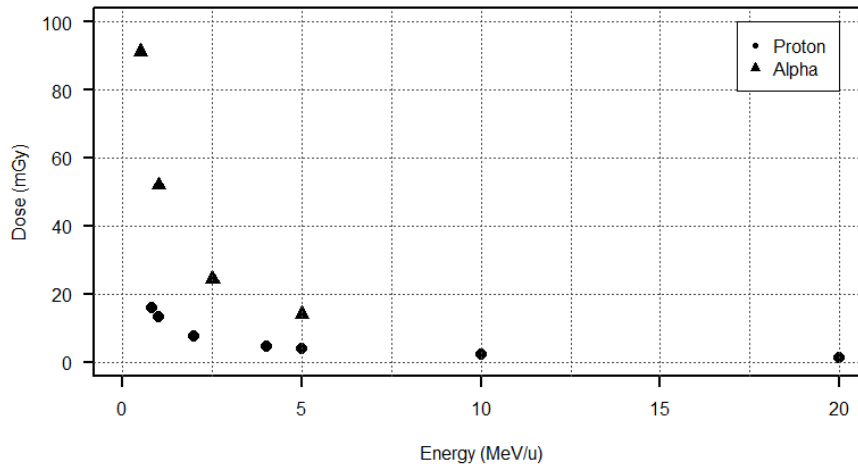


Figure 4.8: Dose of a single track of particle

found to vary with the fractionation used, this is not due to inter-track clustering but to some other mechanism.

4.5 Discussion

The number of DNA breaks can be significantly different when comparing between various incident radiation qualities. Basically, simulations rely on many parameter definitions which can be defined based on the experimental data. Therefore, obtaining the actual number of DNA damage is challenging for several reasons:

- it is difficult to accurately determine event-by-event interactions of a low kinetic energy electron especially below 100 eV due to the uncertainty of position and momentum of the electron.
- apart from ionisation, other processes can also be effective at inducing DNA break below the threshold of ionisation of liquid water. Therefore, chemistry and radiolysis interaction of biomolecule should take into account in the simulation.
- the cross sections available in Geant4-DNA particularly in the version used in this study is of water which further requires accurate cross section for DNA material. The cross sections of biomolecules should be studied in order to accurately mimic biological cells.
- there are a number of adjustable parameters in the modelling of DNA damage including the algorithm for the DNA model, energy threshold for the

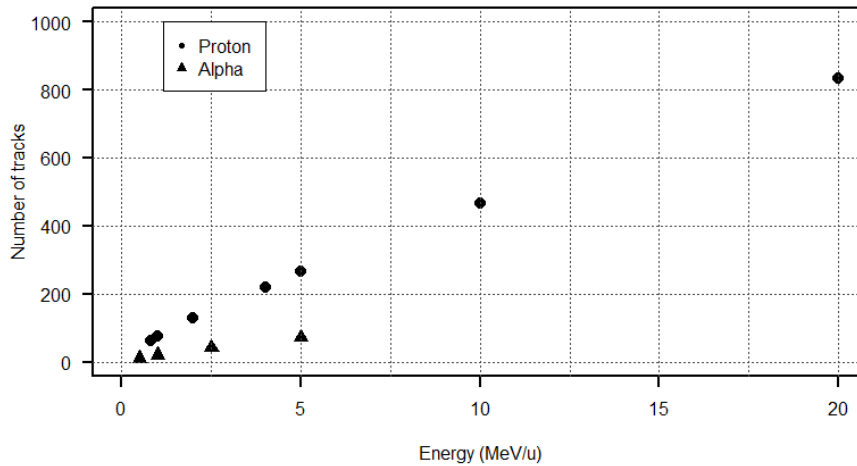


Figure 4.9: Number of tracks for dose 1 Gy

induction of single strand break and the classification of the complexity of DNA damage lesion which varies from one study to another. However, this limitation could be improved by investigating possible factors and constraints that influences the results.

- nucleosome turns, nucleosomes are independent in the DNA model whereas DNA is a long continuous strand. The more complex geometry modelling including the powerful computer would improve the study in the simulation.

Despite these limitations, simulations with Geant4-DNA can be used to produce useful and suggestive results. There are different patterns of DNA strand breaking for protons and for alpha particles; they vary with the particle energy, predictions vary greatly with the energy assumed to be required for a strand break, but there is no great dependence on the fractionation pattern.

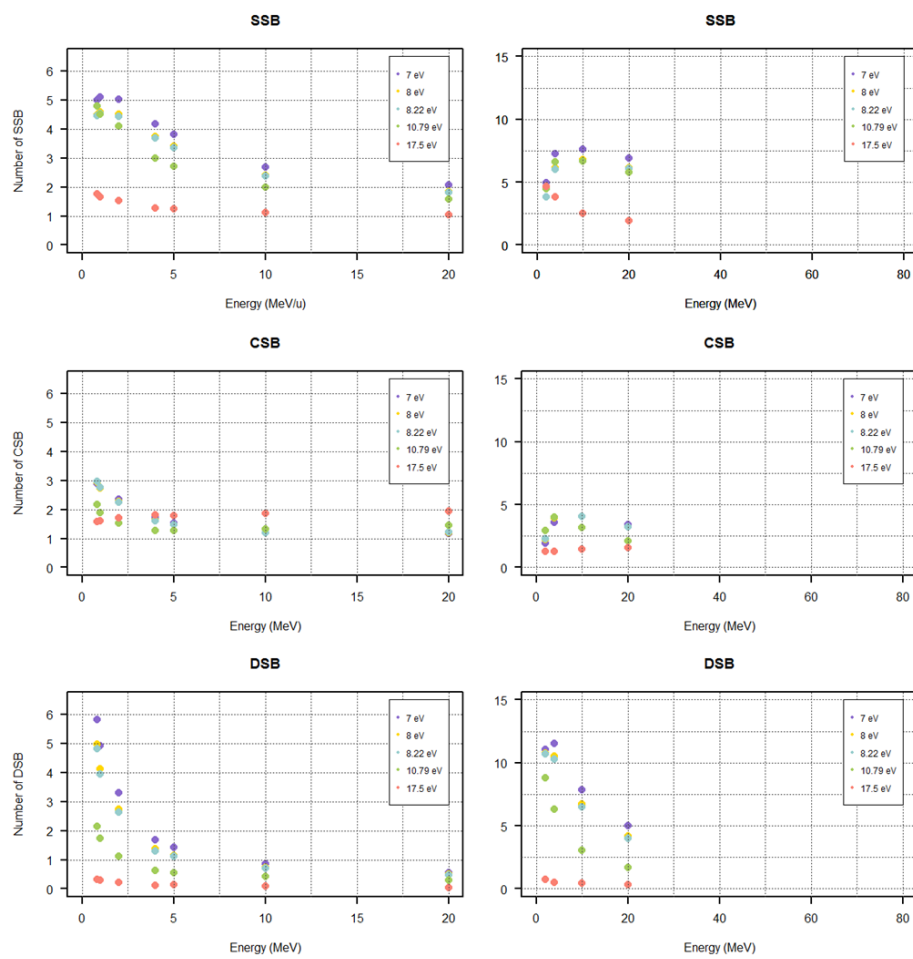


Figure 4.10: Number of DNA break from a single track of proton and alpha particle

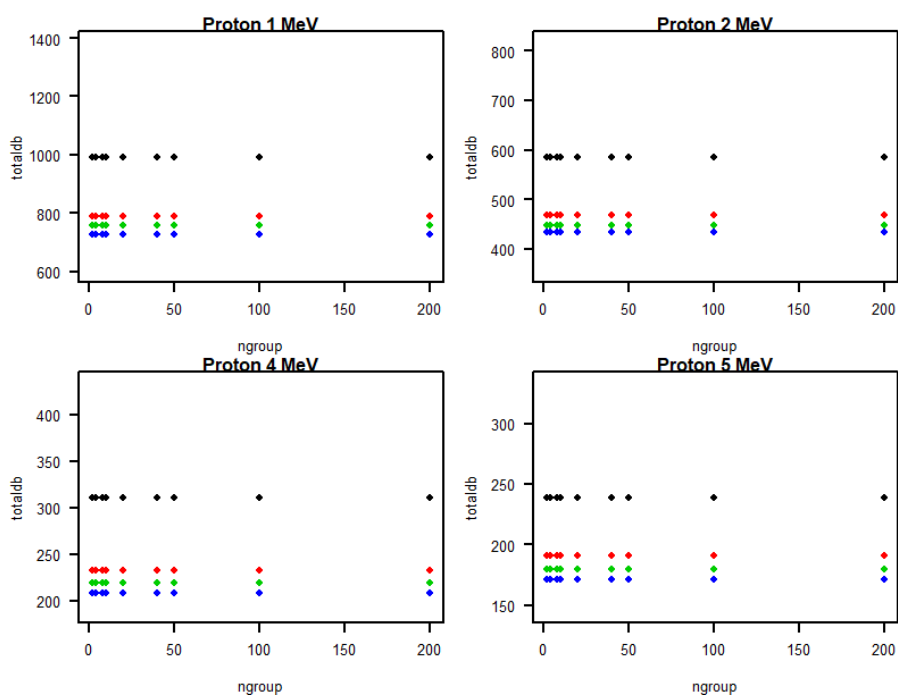


Figure 4.11: Total DNA double strand breaks as a function of a number of tracks in a group. Energy thresholds: black 7 eV, red 8 eV, green 8.22 eV and blue 10.79 eV

Chapter 5

Comparison with data

There have been many useful studies of the effect of radiation, both x-ray and charged particles, in many cell lines using cells in culture. Even though their environment is much simpler than it is in the human body. So that, many important effects for real cancer therapy are not included, they provide much useful information about the effectiveness of possible treatments and the mechanism by which they work.

5.1 The PIDE database

We can investigate how the effectiveness of radiation for killing cells depends on the LET using the cell experiment database, PIDE3 [50]. Experiments *in vitro* on the effect of radiation on living cells are difficult. One has to count the number of cells in the prepared sample, expose it to the desired dose of the desired radiation, and then see how many of them survive. To see whether a cell is alive or dead one has to ascertain whether it is still dividing and reproducing: this takes a considerable time. Furthermore cells die for other reasons, so the numbers have to be normalised using a control sample which is put through the same treatment except for the radiation exposure. Results are accordingly scarce, and the quoted errors are to be treated with care.

The Particle Irradiation Data Ensemble at GSI have compiled a wide and valuable set of experimental data of the effect of irradiation from such experiments. They have made available to us version 3.2 of their database. This includes 1119 different experiments from 115 publications. (2, which seem inconsistent, have been excluded.) There are 21 different particle types ranging from protons to U 92+, with 197 results for protons and 151 for alpha particles. Energies range from 0.26 to 1000 MeV. There are data from 130 different cell lines: the largest number of experiments were done on V79 cells (Chinese Hamsters) with 319 entries, the next most popular are T1 cells with 69. Many cell types have only a single experiment. When considering the number of cell experiments as human cell and non-human cell, there are 557 and 562 entries of data on this database, respectively.

Table 5.1 shows the number of data entries according to type of particle and cell type provided in the database.

Table 5.1: Number of experiments provided by PIDE database

Quantity	Number of experiments
Proton	197
Alpha	151
Higher Z	771
Human cell	557
Non-human cell	562
V 79	319
T1	69
NB1RGB	52
C3H10T1/2	34
Others	645

5.2 RBE and effectiveness

The database includes results on both charged particle and conventional X-ray irradiation. Both are needed to calculate the Relative Biological Effectiveness (RBE) as previously mentioned in section 2.3.3. However we have not used the X-ray data as:

- RBE is not a well-defined universal conversion factor. Even for the same particle charge and energy, the same cell line, and the same X-ray source it varies with the dose. The shapes of the survival curves differ, so if 1 Gy of protons is equivalent to 2 Gy of X-rays, that does not imply that 2 Gy of protons are equivalent to 4 Gy.
- The inclusion of the X-ray data adds another set of the inevitable experimental errors to the results.
- RBE is useful for the many practitioners who are familiar with X-ray procedures and for whom charged particle therapy is new and different, but not for the understanding of the new therapy in its own right. It is analogous to using horsepower to describe an electric motor.

5.3 LET

The PIDE database includes the LET for the experiment. However, this value is sometimes taken from the experiment and sometimes calculated from a simulation

program. In order to eliminate inconsistencies between experiments, we would like to use the same definition for all of them. We have, therefore, calculated the Bethe-Bloch value for particles of the given charge and energy. These are shown in Figure 5.1A.

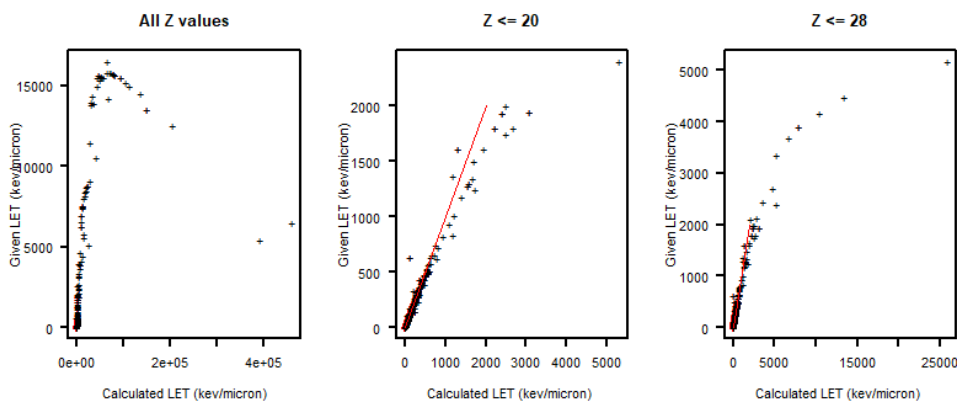


Figure 5.1: Calculated and given LET values for (a) all data and (b) those with $Z \leq 20$ and (c) those with $Z \leq 28$: the red line is the line of equality.

At high values there is serious disagreement which is not understood. These come from the experiments with high z particles. Restricting the selection to low z gives Figure 5.1B, and the agreement is reasonable. We therefore restrict the data used to these values, and can use our calculated LET values for consistency.

5.4 Dose-survival curves

For some of the experiments only the LQ α and β values are quoted, but for 954 experiments the data is given. On inspection, these are generally well described by a single exponential model. This is shown in Figure 5.2, for four of the experiments taken at random. The fits shown are the straight line fit to the logarithm, $\log(S) = mD + c$, in black, and the one parameter straight line through the origin, $\log(X) = mD$, in red. The quadratic fit is in green. There is little evidence for non-linear behaviour. This is known to be less important for charged particles than it is for X-rays [51].

This is further justified by the β values give in the PIDE database, as shown in Figure 5.4. This shows their calculated values and the ones quoted in the original papers. It can be seen that the values are generally small, and the two versions are often in disagreement.

We have performed quadratic fit and examined the effect by comparing the slop from the linear fit with the averaged slop from the quadratic fit which we take as the survival fraction at the mean dose. The plot is

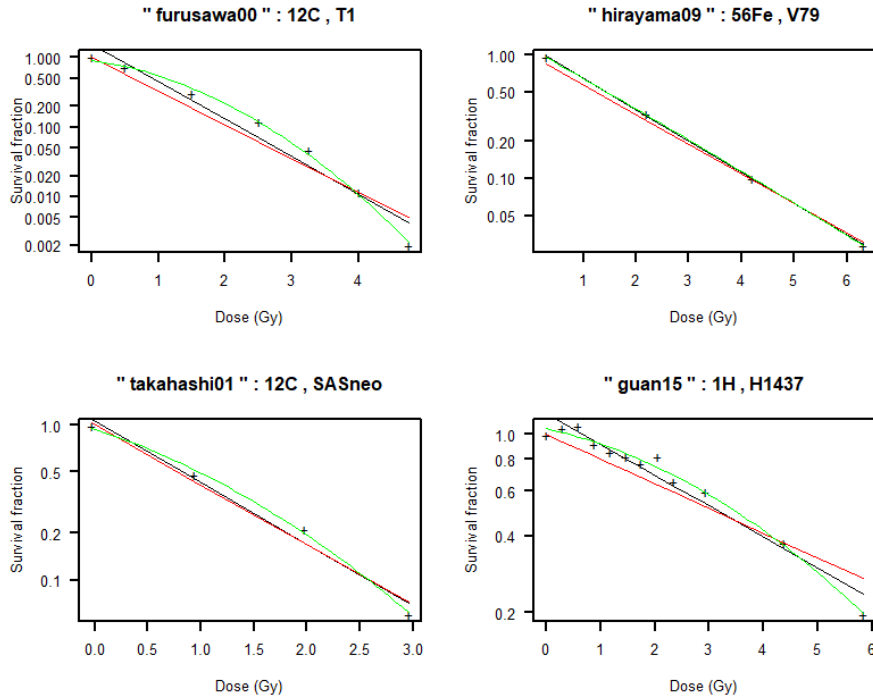


Figure 5.2: Four experimental data of the 954 datasets. The title of each plot is given as: "Author and year of publication": type of particle, type of cell used in the study. The lines are described in the text

We therefore neglect the quadratic term, and use the single parameter fits, as we would expect 100% survival at zero dose, in the absence of any 'plating term'. Experiments with large fitted values of c have been examined and do not appear anomalous.

The experimental errors on the data points are not given. To improve this will require a proper study of how such errors arise. They are binomial in principle, which would make the errors greatest in the middle of the graph, but the subtraction of the control (unirradiated) sample introduces a further complication. Thus, for the present all points are given equal weight in the fit.

By analogy with the RBE one can introduce the 'Absolute Biological Effectiveness' or ABE. This term is used as working title only as there are previous definitions in other works[52, 53].

D. Watt [54] suggested in 1989 that RBE and LET_i have fundamental physical limitation in determining biological damage process. Absolute biological effectiveness was consequently defined to refer as a unified parameter without knowledge of the radiation type or intensity.

$$ABE = \sigma_i \phi_{s,i}$$

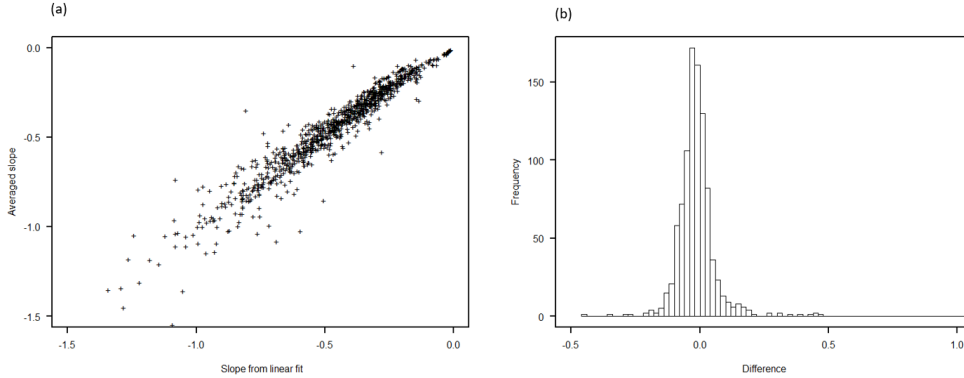


Figure 5.3: The difference of linear and quadratic fit through survival fraction and delivered dose of V79 cell data sets. a) a relationship of slope from linear fit and averaged fit b) a histogram showing the difference between slope from linear fit and averaged fit

where σ_i is the cross section for the effect of interest and $\phi_{s,i}$ is the flux of the charged particles including secondary electron and other radiation that cause the damage. This is similar to our definition because it is no comparison of photon as a reference but it is a definition in terms of mechanism where as our definition is purely descriptive.

More recently, ABE was proposed by K. Ono et al [53] in order to properly evaluate the dose required in the treatment which accurately relate to its biological effect to tumour cells. The ABE factor is based on the investigation of radiosensitivity of tumour cells to $^{10}\text{B}(n,\alpha)^7\text{Li}$.

$$ABE \text{ factor} = Gy/D_0$$

where D_0 is the dose that gives 37% survival rate. The ABE dose can be calculated by multiplying ABE factor by the physical dose. This means the dose that can decrease the cell survival rate to $e^{-ABE \text{ dose}/Gy}$. This is similar to our definition although it is complicated because they use it for boron neutron capture therapy (BNCT) and need to include the relationship between the neutron flux and the LET, which depends on the boron concentration.

The RBE is the reciprocal of the dose required for a particular mortality, and for a simple exponential this is just the slope. We therefore use

$$ABE \equiv -\alpha \quad (5.1)$$

Figure 5.5a shows all the ABE values obtained, as a function of the LET predicted by the Bethe-Bloch formula. There is considerable variation of ABE with LET. It increases to a peak around 150 keV/ μm and then falls off slowly (the 'overkill effect'). The peak is shown in more detail in figure 5.5b

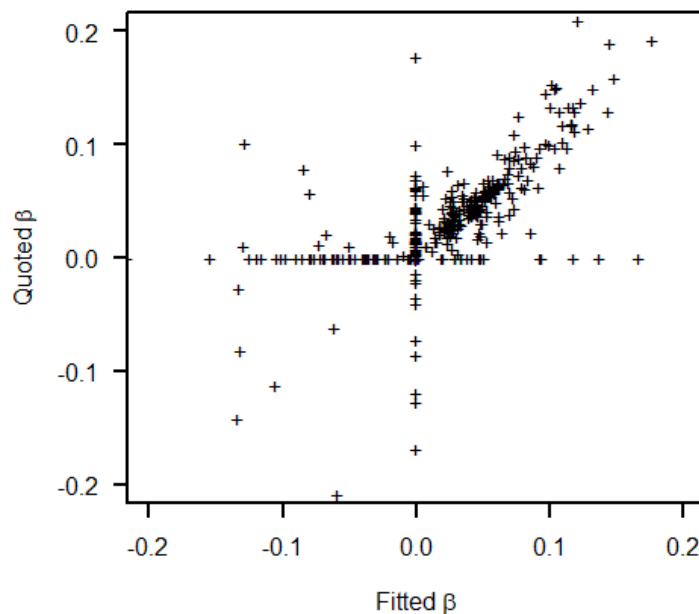


Figure 5.4: Fitted and quoted values of β , taken from the PIDE database

There is considerable spread of points about the trend. Some of this is due to experimental error. Some of it is presumably due to difference in the cell type.

5.5 Dependence on cell type

This is studied in figure 5.6 which shows the subsets of the data for the V79, T1, C3H10T1 and NB1RGB cells. The behaviour does indeed appear to be different for each cell type, as one would expect. However, there is no clear systematic difference between human and non-human cells. Plot ABE against LET for four cell types. They are 4 most of the entries of the cells available in the database. We restricted LET to below $200 \text{ keV}/\mu\text{m}$ because we can fit it by the parabola. If we go above $200 \text{ keV}/\mu\text{m}$, the parabola does not give a good fit.

Extending to the cubic and quartic does improve the fit but introduces features which are obviously spurious. It would be interesting to try fit to other simple forms perhaps motivated by model of over kill.

The coefficient of the parabolic fit are given in the table 5.2.

We have 4 sets of parameters that show the same pattern but they are not exactly the same.

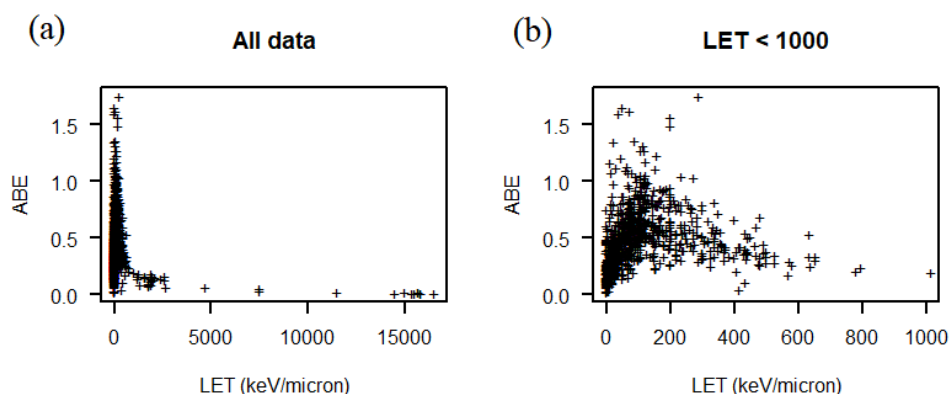


Figure 5.5: Fitted values of the negated slope plotted against the LET obtained from the Bethe-Bloch formula. a) all cell lines and b) LET is restricted to less than 1000 keV/ μ m

Table 5.2: Coefficient of parabolic fit of four cell types

Cell type	Constant	Linear	Quadratic
V79	0.125	0.0071	-2.89×10^{-5}
T1	0.136	0.0074	-2.92×10^{-5}
C3H10T1/2	0.105	0.0094	-3.81×10^{-5}
NB1RGB	0.222	0.0079	-2.54×10^{-5}

5.6 Dependence on particle type

Some of the differences in figure 5.5 may be due to difference in particle species. For the V79 cells the results for protons, alpha particles and other ions are shown in different colours in figure 5.7: the T1 results are almost all from high z particles. It can be obviously noticed that the ABE values of V79 cell as a function of LET rise and fall similar to the RBE value. This fall represents the overkill effect. However, using ABE does not require to compare to reference radiation or photon dose which would add another error to the results.

It is an interesting question as to whether, say, protons and alpha particles with different energies but the same LET have the same effectiveness[55, 47]. This is hard to study as most proton beams have lower LET than most alpha beams. The figure 5.7 indicates that there is some overlap for LET values below 100 keV/ μ m, and these are shown in figure 5.8 together with a straight line fit through all data points. If the deviations of the points from the line are taken separately for protons, alphas, and higher z particles, as shown in figure 5.9, the values are

When looking at figure 5.9 the proton histogram appears central, whereas that for alpha has a positive mean and for the higher z value it is negative. This is

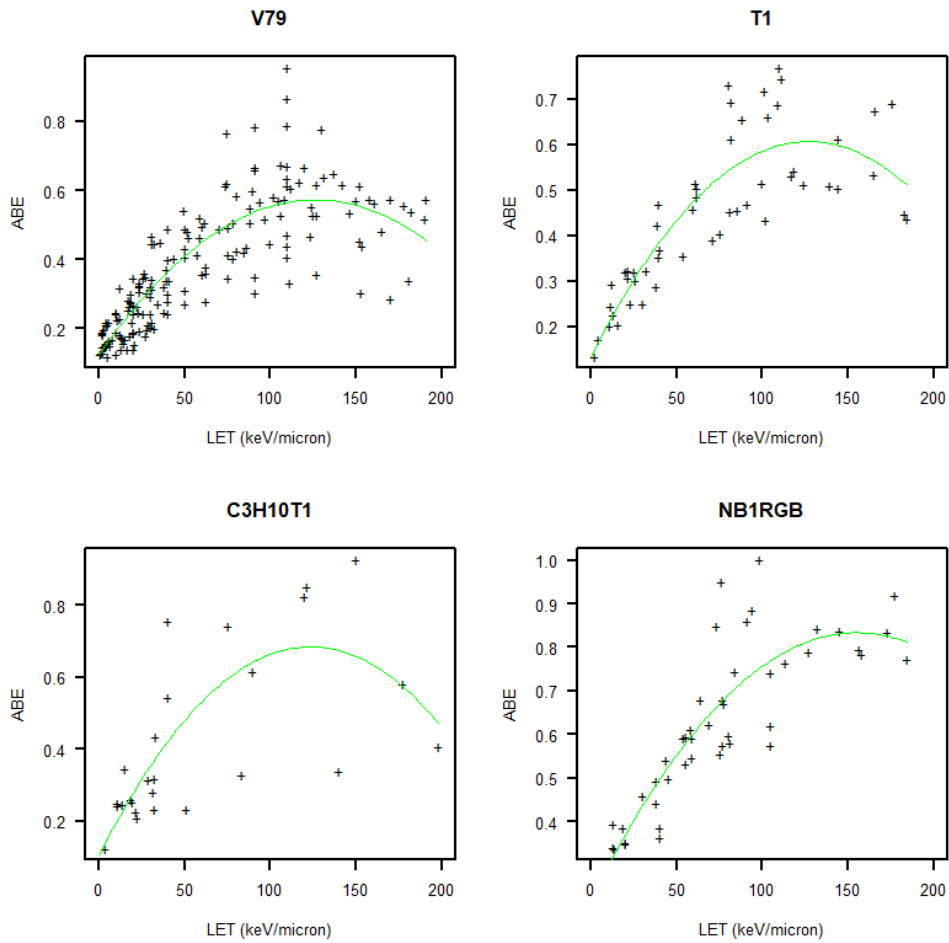


Figure 5.6: The parabolic fit of ABE as a function of LET ($\text{keV}/\mu\text{m}$) of V79, T1, C3H10T1 and NB1RGB cells

supported by calculating the mean of each sub-sample as shown in table 5.3 which gives the means and the associated error, as calculated from the standard deviation divided by the square of root of the number of entries. The alpha particle values do indeed lie above the overall average with a significance of 2.22σ this has a p-value of 0.026 so that there is only 2.6 % chance of this happening naturally. However, the heavy ion data lies below the average by 3.88σ and there is only 0.01 % probability that this could happen naturally.

Although, the data clearly shows this difference in behaviour in the data between low charged and high charged ions, there could be several explanations. Different ions may have been used by different experiments with different techniques giving different systematic effect. Nevertheless it is very suggestive and should be studied further.

Table 5.3: Deviation from the straight line for 3 particle types for the V79 sample

Particle	Deviation from fit	significance	p -value
proton	0.0063 ± 0.0086	0.73σ	0.46
alpha	0.0379 ± 0.0170	2.22σ	0.026
$z > 2$ ions	-0.0399 ± 0.0103	3.88σ	0.00010

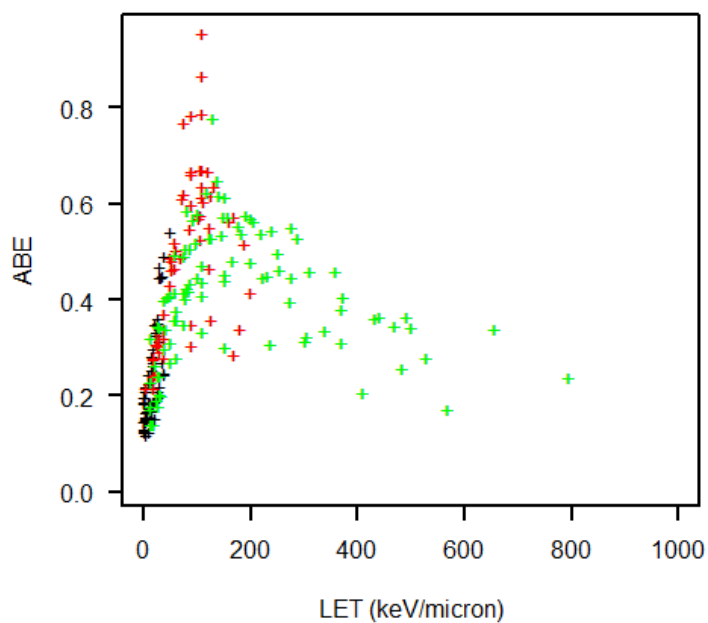


Figure 5.7: The ABE values of V79 cell as a function of LET (black crosses: proton, red: alpha , green: particle at z higher than 2)

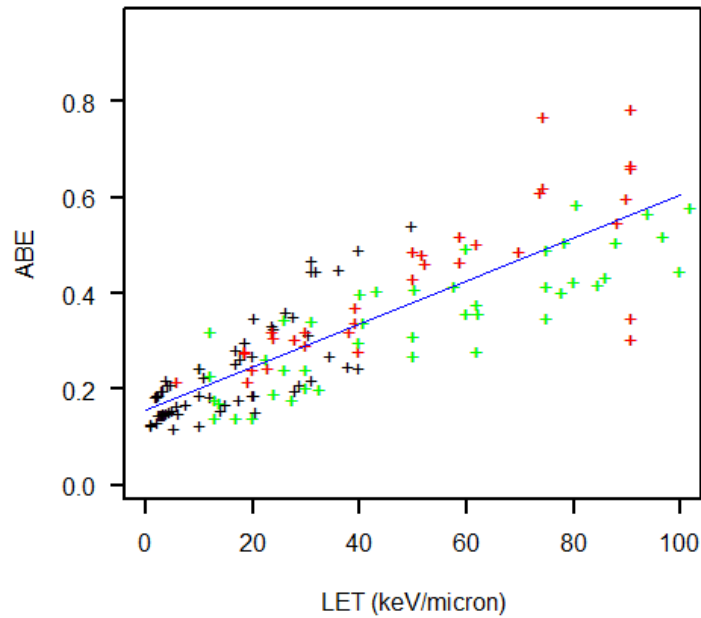


Figure 5.8: The ABE values of V79 cell as a function of LET (LET is restricted to $100 \text{ keV}/\mu\text{m}$). Black crosses: proton, Red: alpha , green: particle at z higher than 2. The blue straight line represent the line of regression through all the data

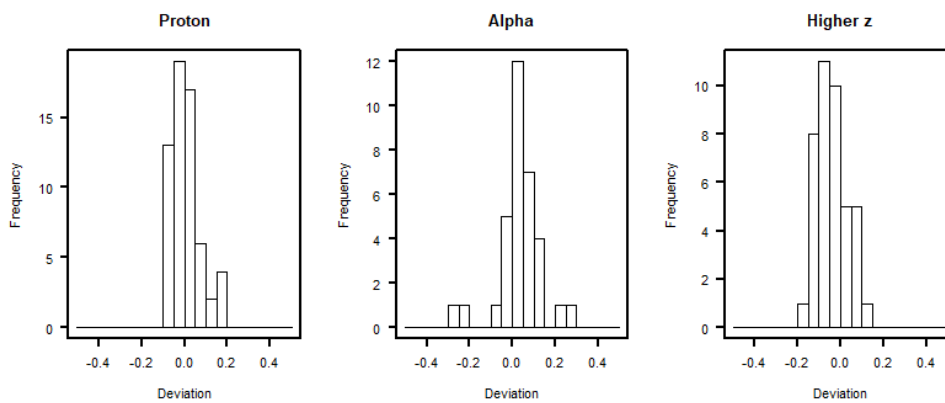


Figure 5.9: Histogram of three different particles showing the deviation of the points from the straight regression line in figure 5.8

Chapter 6

Conclusion

6.1 Conclusion

There are currently proton and hadron therapy centres opening across the world which shows the increase of treating cancer with charged particles because of their distinct dose distribution. However, we have only limited experience on the biological outcomes that may arise from charged particle beams. This is partly because of the ethical issue that we cannot do the experiment on humans and partly of the complicated processes involved in biological environment.

In fact, we have been developing and improving the treatment for charged particles from experiences based on X-ray by converting known X-ray dose to a factor of dose given by other types of radiation. Because of the stochastic nature of the radiation, this converting factor cannot be obtained directly. A number of factors may influence the outcome of cell killing including physical properties of charged particle, interaction of the particle to the biomaterial inside the cell. Therefore, it is challenging to determine these factors in more detail.

There is a good understanding of the way charged particles lose their energies in material. This is due to the knowledge of particle physics which is encapsulated in Bethe-Bloch formula, Landau distribution and Geant4 simulation.

The definition of LET may seem simple but in practical the calculation of LET can differ in what meant by energy deposition and distance. Currently, both of energy deposition and distance of the charged particle beam cannot be measured directly from the experiment. Instead, we calculate them based on our physics knowledge. Therefore, the method in which we derive these important values in order to get correct LET can make substantial difference. This thesis has applied such knowledge to proton and alpha particle by exploring the difference between LET_t and LET_d , the number of DNA breaks of different types in different condition by using Geant4 simulation. What could be highlighted from this study is that target scale or target size is really important in LET_d calculation and the appropriate value should be properly defined.

We have seen that the number of strand breaks, which is presumed to be

strongly linked to cell mortality, can be predicted. It depends on the particle type and energy and also on the energy required to break a DNA strand. Any dependence on fractionation appears to be very weak. We have considered *in vitro* experiment from PIDE database in the light of this approach and have found that the indication of difference between different ions that goes beyond different in their LET

6.2 Future development

A main limitation of radiation transport and track structure codes is focus on the physical events and limited tracking of chemical and biological effects which is more complex in cell environment. Despite these limitations, studies such as this one can yield suggestive results. A future continuation should include the proper treatment of several points.

In discussing, LET_t and LET_d we need to investigate what scale would be appropriate for LET_d

In this study, only direct physical interaction was included so the number of breaks would differ significantly if the indirect effect was considered

The study of PIDE does not consider the errors of the data points. To incorporate these will require referring the original publications. We hope that these steps can be achieved, and further useful insights and predictions obtained as a result.

Bibliography

- [1] J. Allison, K. Amako, J. Apostolakis, H. Araujo, P. A. Dubois, M. Asai, G. Barrand, R. Capra, S. Chauvie, R. Chytracsek, G. A. P. Cirrone, G. Cooperman, G. Cosmo, G. Cuttone, and Daquino, “Geant4 developments and applications,” *IEEE Transactions on Nuclear Science*, vol. 53, no. 1, pp. 270–278, 2006.
- [2] domdomegg, “A simple diagram of an unspecialised animal cell,” 2016.
- [3] “Cell cycle overview.”
- [4] I. El Naqa, P. Pater, and J. Seuntjens, “Monte Carlo role in radiobiological modelling of radiotherapy outcomes,” *Phys Med Biol*, vol. 57, no. 11, pp. R75–97, 2012.
- [5] H. Paganetti, “Significance and implementation of RBE variations in proton beam therapy,” *Technology in cancer research & treatment*, vol. 2, no. 5, pp. 413–426, 2003.
- [6] PTCOG, “Particle therapy facilities under construction,” 2019. Last accessed 15 February 2020.
- [7] S. cancer care alliance, “Look behind the gantry.”
- [8] H. Paganetti, A. Niemierko, M. Ancukiewicz, L. E. Gerweck, M. Goitein, J. S. Loeffler, and H. D. Suit, “Relative biological effectiveness (rbe) values for proton beam therapy,” *International Journal of Radiation Oncology*Biology*Physics*, vol. 53, no. 2, pp. 407 – 421, 2002.
- [9] M. A. Hill, “Track to the future: historical perspective on the importance of radiation track structure and DNA as a radiobiological target,” *Int J Radiat Biol*, vol. 94, no. 8, pp. 759–768, 2018.
- [10] T. R. Munro, “The relative radiosensitivity of the nucleus and cytoplasm of chinese hamster fibroblasts,” *Radiation Research*, vol. 42, no. 3, pp. 451–470, 1970.

- [11] Z. Francis, C. Villagrasa, and I. Clairand, "Simulation of DNA damage clustering after proton irradiation using an adapted DBSCAN algorithm," *Comput Methods Programs Biomed*, vol. 101, no. 3, pp. 265–70, 2011.
- [12] S. Meylan, S. Incerti, M. Karamitros, N. Tang, M. Bueno, I. Clairand, and C. Villagrasa, "Simulation of early DNA damage after the irradiation of a fibroblast cell nucleus using Geant4-DNA," *Sci Rep*, vol. 7, no. 1, p. 11923, 2017.
- [13] N. Lampe, M. Karamitros, V. Breton, J. M. C. Brown, D. Sakata, D. Sarramia, and S. Incerti, "Mechanistic DNA damage simulations in Geant4-DNA part 2: Electron and proton damage in a bacterial cell," *Phys Med*, vol. 48, pp. 146–155, 2018.
- [14] F. M. Khan, J. Gibbons, John P., J. Pine, Jonathan W., E. Moyer, A. Jackson, J. Clements, and J. Wendt, *Khan's the physics of radiation therapy*. Philadelphia, Pennsylvania: Wolters Kluwer, fifth ed., 2014.
- [15] W. D. Newhauser and R. Zhang, "The physics of proton therapy," *Physics in Medicine and Biology*, vol. 60, pp. R155–R209, Mar 2015.
- [16] M. Tanabashi, K. Hagiwara, K. Hikasa, and Nakamura, "Review of particle physics," *Phys. Rev. D*, vol. 98, p. 030001, Aug 2018.
- [17] L. Landau, "On the energy loss of fast particles by ionization," *J. Phys.(USSR)*, vol. 8, pp. 201–205, 1944.
- [18] D. H. Wilkinson, "Ionization energy loss by charged particles part i. the Landau distribution," *Nuclear Instruments and Methods in Physics Research Section A: Accelerators, Spectrometers, Detectors and Associated Equipment*, vol. 383, no. 2, pp. 513–515, 1996.
- [19] H. H. Rossi and M. Zaider, *Microdosimetry and its applications*. Berlin: Springer, 1996.
- [20] E. J. Hall and A. J. Giaccia, *Radiobiology for the radiologist: Seventh edition*, pp. 1–576. Radiobiology for the Radiologist: Seventh Edition, 2012. Cited By :24.
- [21] Z. Francis and A. Stypczynska, *Clustering algorithms in radiobiology and DNA damage quantification*. 2013.
- [22] L. De Nardo, P. Colautti, W. Y. Baek, B. Grosswendt, A. Alkaa, P. Ségur, and G. Torielli, "Track nanodosimetry of an alpha particle," *Radiation Protection Dosimetry*, vol. 99, no. 1-4, pp. 355–358, 2002.
- [23] G. Garty, S. Shchemelinin, A. Breskin, R. Chechik, G. Assaf, I. Orion, V. Bashkirov, R. Schulte, and B. Grosswendt, "The performance of a novel

- ion-counting nanodosimeter,” *Nuclear Instruments and Methods in Physics Research Section A: Accelerators, Spectrometers, Detectors and Associated Equipment*, vol. 492, no. 1, pp. 212–235, 2002.
- [24] A. Jansen and K. J. Verstrepen, “Nucleosome positioning in *saccharomyces cerevisiae*,” *Microbiol Mol Biol Rev*, vol. 75, no. 2, pp. 301–20, 2011.
- [25] J. L. T. Jeremy M Berg and L. Stryer, *Biochemistry 5th edition*. New York: W H Freeman, 2002.
- [26] B. R. Wood, “The importance of hydration and dna conformation in interpreting infrared spectra of cells and tissues,” *Chem. Soc. Rev.*, vol. 45, pp. 1980–1998, 2016.
- [27] A. T. Annunziato, “DNA packaging: Nucleosomes and chromatin.,” *Nature Education*, vol. 1(1):26, 2008.
- [28] D. Frankenberg, M. Frankenberg-Schwager, D. Blöcher, and R. Harbich, “Evidence for DNA double-strand breaks as the critical lesions in yeast cells irradiated with sparsely or densely ionizing radiation under oxic or anoxic conditions,” *Radiation Research*, vol. 88, no. 3, pp. 524–532, 1981.
- [29] D. T. Goodhead, “Initial events in the cellular effects of ionizing radiations: Clustered damage in DNA,” *International Journal of Radiation Biology*, vol. 65, no. 1, pp. 7–17, 1994.
- [30] P. L. Olive, “The role of DNA single- and double-strand breaks in cell killing by ionizing radiation,” *Radiation Research*, vol. 150, no. 5, pp. S42–S51, 1998.
- [31] R. Amunugama and R. Fishel, *Chapter 7 - Homologous Recombination in Eukaryotes*, vol. 110, pp. 155–206. Academic Press, 2012.
- [32] H. Paganetti, *Proton Therapy Physics*. Taylor & Francis / CRC Press, 2012.
- [33] F. Romano, G. A. P. Cirrone, G. Cuttone, F. D. Rosa, S. E. Mazzaglia, I. Petrovic, A. R. Fira, and A. Varisano, “A Monte Carlo study for the calculation of the average linear energy transfer (LET) distributions for a clinical proton beam line and a radiobiological carbon ion beam line,” *Physics in Medicine and Biology*, vol. 59, no. 12, pp. 2863–2882, 2014.
- [34] M. A. Cortés-Giraldo and A. Carabe, “A critical study of different Monte Carlo scoring methods of dose average linear-energy-transfer maps calculated in voxelized geometries irradiated with clinical proton beams,” *Physics in Medicine and Biology*, vol. 60, no. 7, pp. 2645–2669, 2015.

- [35] S. Incerti, G. Baldacchino, M. Bernal, R. Capra, C. Champion, Z. Francis, P. Guèye, A. Mantero, B. Mascialino, P. Moretto, P. Nieminen, C. Villagrasa, and C. Zacharatou, “The Geant4-DNA project,” *International Journal of Modeling, Simulation, and Scientific Computing*, vol. 01, no. 02, pp. 157–178, 2010.
- [36] S. Incerti, A. Ivanchenko, M. Karamitros, A. Mantero, P. Moretto, H. N. Tran, B. Mascialino, C. Champion, V. N. Ivanchenko, M. A. Bernal, Z. Francis, C. Villagrasa, G. Baldacchino, P. Guèye, R. Capra, P. Nieminen, and C. Zacharatou, “Comparison of Geant4 very low energy cross section models with experimental data in water,” *Medical Physics*, vol. 37, no. 9, pp. 4692–4708, 2010.
- [37] S. Incerti, M. Psaltaki, P. Gillet, P. Barberet, M. Bardiès, M. A. Bernal, M. C. Bordage, V. Breton, M. Davidkova, E. Delage, Z. El Bitar, Z. Francis, S. Guatelli, A. Ivanchenko, V. Ivanchenko, M. Karamitros, S. B. Lee, L. Maigne, S. Meylan, K. Murakami, P. Nieminen, H. Payno, Y. Perrot, I. Petrovic, Q. T. Pham, A. Ristic-Fira, G. Santin, T. Sasaki, H. Seznec, J. I. Shin, V. Stepan, H. N. Tran, and C. Villagrasa, “Simulating radial dose of ion tracks in liquid water simulated with Geant4-DNA: A comparative study,” *Nuclear Instruments and Methods in Physics Research Section B: Beam Interactions with Materials and Atoms*, vol. 333, pp. 92–98, 2014.
- [38] F. Guan, C. Peeler, L. Bronk, C. Geng, R. Taleei, S. Randeniya, S. Ge, D. Mirkovic, D. Grosshans, R. Mohan, and U. Titt, “Analysis of the track- and dose-averaged LET and LET spectra in proton therapy using the Geant4 Monte Carlo code,” *Medical Physics*, vol. 42, no. 11, pp. 6234–6247, 2015.
- [39] R. Grün, T. Friedrich, E. Traneus, and M. Scholz, “Is the dose-averaged LET a reliable predictor for the relative biological effectiveness?,” *Medical Physics*, vol. 46, no. 2, pp. 1064–1074, 2019.
- [40] I. Radulescu, K. Elmroth, and B. Stenerlöw, “Chromatin organization contributes to non-randomly distributed double-strand breaks after exposure to high-LET radiation,” *Radiation Research*, vol. 161, no. 1, pp. 1–8, 8, 2004.
- [41] M. Dos Santos, C. Villagrasa, I. Clairand, and S. Incerti, “Influence of the DNA density on the number of clustered damages created by protons of different energies,” *Nuclear Instruments and Methods in Physics Research Section B: Beam Interactions with Materials and Atoms*, vol. 298, pp. 47–54, 2013.
- [42] P. Pater, G. Bäckström, F. Villegas, A. Ahnesjö, S. A. Enger, J. Seuntjens, and I. El Naqa, “Proton and light ion RBE for the induction of direct DNA double strand breaks,” *Medical Physics*, vol. 43, no. 5, pp. 2131–2140, 2016.

- [43] N. Tang, M. Bueno, S. Meylan, S. Incerti, H. N. Tran, A. Vaurijoux, G. Gruel, and C. Villagrasa, “Influence of chromatin compaction on simulated early radiation-induced DNA damage using Geant4-DNA,” *Medical Physics*, vol. 46, no. 3, pp. 1501–1511, 2019.
- [44] M. Ester, H.-P. Kriegel, J. Sander, and X. Xu, *A density-based algorithm for discovering clusters a density-based algorithm for discovering clusters in large spatial databases with noise*. Proceedings of the Second International Conference on Knowledge Discovery and Data Mining, Portland, Oregon: AAAI Press, 1996.
- [45] H. R. Drew, R. M. Wing, T. Takano, C. Broka, S. Tanaka, K. Itakura, and R. E. Dickerson, “Structure of a B-DNA dodecamer: conformation and dynamics,” *Proceedings of the National Academy of Sciences of the United States of America*, vol. 78, no. 4, pp. 2179–2183, 1981.
- [46] P. Pater, J. Seuntjens, I. El Naqa, and M. A. Bernal, “On the consistency of Monte Carlo track structure DNA damage simulations,” *Medical Physics*, vol. 41, no. 12, p. 121708, 2014.
- [47] N. T. Henthorn, J. W. Warmenhoven, M. Sotiropoulos, R. I. Mackay, K. J. Kirkby, and M. J. Merchant, “Nanodosimetric simulation of direct ion-induced DNA damage using different chromatin geometry models,” *Radiation Research*, vol. 188, no. 6, pp. 770–783, 14, 2017.
- [48] B. H. Lee and C. K. C. Wang, “A cell-by-cell Monte Carlo simulation for assessing radiation-induced DNA double strand breaks,” *Physica Medica*, vol. 62, pp. 140–151, 2019.
- [49] L. de la Fuente Rosales, S. Incerti, Z. Francis, and M. A. Bernal, “Accounting for radiation-induced indirect damage on DNA with the geant 4-DNA code,” *Physica Medica*, vol. 51, pp. 108–116, 2018.
- [50] T. Friedrich, U. Scholz, T. Elsässer, M. Durante, and M. Scholz, “Systematic analysis of RBE and related quantities using a database of cell survival experiments with ion beam irradiation,” *Journal of radiation research*, vol. 54, no. 3, pp. 494–514, 2013.
- [51] S. J. McMahon, “The linear quadratic model: usage, interpretation and challenges,” *Physics in Medicine & Biology*, vol. 64, no. 1, p. 01TR01, 2018.
- [52] D. Watt, “Absolute biological effectiveness of neutrons and photons,” *Radiation Protection Dosimetry*, vol. 23, no. 1-4, pp. 63–67, 1988.
- [53] K. Ono, H. Tanaka, Y. Tamari, T. Watanabe, M. Suzuki, and S.-I. Masunaga, “Proposal for determining absolute biological effectiveness of boron neutron

capture therapy-the effect of $^{10}\text{B}(n,\alpha)^7\text{Li}$ dose can be predicted from the nucleocytoplasmic ratio or the cell size,” *Journal of radiation research*, vol. 60, no. 1, pp. 29–36, 2019.

[54] D. E. Watt, “On absolute biological effectiveness and unified dosimetry,” *Journal of Radiological Protection*, vol. 9, pp. 33–49, mar 1989.

[55] D. T. Goodhead, *Particle Track Structure and Biological Implications*, pp. 1–21. Cham: Springer International Publishing, 2018.